Table 1
Characteristic genes expressed in CH-B-related HCC.

Genes	Symbol	GenBank ID	Cluster No.	Up- or down-regulated	GO
Placental growth factor, vascular endothelial growth factor-related protein	PGF	NM_002632	8	Up	Angiogenesis
Telomerase-associated protein 1	TEP1	NM_007110	8	Up	Telomere maintenance
Stathmin 1/oncoprotein 18	STMN1	J04991	8	Up	Microtubule depolymerization
SUMO-1 activating enzyme subunit 2	UBA2	NM_005499	9	Up	Protein modification process
Cyclin E1	CCNE1	NM_001238	9	Up	Cell cycle
V-myc myelocytomatosis viral related oncogene	MYCN	NM_005378	9	Up	Regulation of transcription from RNA polymerase II promoter
Glypican 3	GPC3	NM_004484	9	Up	Anatomical structure morphogenesis
Midkine (neurite growth-promoting factor 2)	MDK	NM_002391	9	Up	Cell differentiation
Collagen, type IV, alpha 1	COL4A1	NM_001846	9	Up	Extracellular matrix structural constituent
Gamma-aminobutyric acid (GABA) A receptor	GABRE		11	Up	ion transport
Thrombospondin 2	THBS2	NM_003247	11	Up	Cell adhesion
Transferrin receptor (p90, CD71)	TrF1	AW025110	11	Up	Cellular iron ion homeostasis
Baculoviral IAP repeat containing 5 (Survivin)	BIRC5	NM_001168	11	Up	cytokinesis
Ornithine aminotransferase	OAT	NM_000274	12	Down	Transaminase activity
Insulin receptor substrate 1	IRS1	NM_005544	12	Down	Positive regulation of mesenchymal cell proliferation
Glutamate dehydrogenase 2	GLUD2	NM_012084	12	Down	Cellular amino acid metabolic process
Acyl-CoA oxidase 2	ACOX2	NM_003500	12	Down	Lipid metabolic process
Insulin-like growth factor 2 receptor	IGF-2R	AL353625	13	Down	Transport
Leukocyte cell-derived chemotaxin 2	LECT2, IL-9	AC002428	13	Down	System development
Hydroxysteroid (11-beta) dehydrogenase 1	HSD11B1	NM_181755	13	Down	Lipid metabolic process
Diablo, IAP-binding mitochondrial protein	DIABLO	NM_019887	13	Down	Induction of apoptosis
Cytochrome P450, family 39, subfamily A, polypeptide 1	CYP39A1	NM_016593	13	Down	Bile acid biosynthetic process
N-acetyltransferase 2	NAT-2	NM_000015	13	Down	Metabolic process
Solute carrier family 39 (zinc transporter), member 14	SLC39A14	NM_015359	13	Down	Ion transport
Acetyl-coenzyme A acyltransferase 2	ACAA2	NM_006111	16	Down	Lipid metabolic process

2.4. Framework of gene clusters in relation to hepatocarcinogenesis of CH-B using GGM

We used GGM to examine the relationship between non-cancerous and HCC gene clusters. The partial correlation coefficient matrix (PCCM) generated by GGM is shown in Supplemental Tables H and I. The frame networks of genetic clusters are shown in Fig. 3. The blue lines indicate a negative partial correlation and the black lines indicate a positive partial correlation. Multiple correlations were observed within the non-cancerous and HCC clusters. In addition, some interesting correlations between non-cancerous and HCC clusters were noted. In CH-B (Fig. 3A), non-cancerous cluster No. 3 was up-regulated and correlated with HCC cluster Nos. 8 and 18. Non-cancerous cluster No. 3 was composed of wnt signaling and oxidative stress-related genes, HCC cluster No. 8 was composed of VEGF family signaling-related genes, and HCC cluster No. 18 was composed of estrogen receptor 1 (ESR1) regulation of G1/S transition-related genes. Moreover, non-cancerous cluster No. 16 correlated positively with HCC cluster No. 11 and negatively with HCC cluster No. 18. Non-cancerous cluster No. 16 was composed of cytokine production and apoptosis-related genes, while HCC cluster No. 11 was composed of apoptosis and survival-related genes. The down-regulated non-cancerous cluster No. 13 in CH-B correlated negatively with HCC cluster No. 8. Non-cancerous cluster No. 13 was composed of hepatic functional genes, such as those related to cholesterol metabolism and the TCA cycle.

The correlations between these clusters were further confirmed by examining individual gene interactions with reference to the MetaCore database (Fig. 4A). Eight genes in non-cancerous cluster Nos. 3 and 16 were directly associated with AP1 in HCC cluster No. 18. These genes are related to development and the DNA damage response. In HCC cluster No. 18, many of the cell cycle, development, immune system, and metabolism-related genes were regulated by AP1 [18–20]. In addition, it is interesting to note that the HBV transcript clustered in HCC cluster No. 18 (Fig. 1). The up-regulated HCC cluster No. 11 was associated with AP1 [21]. In addition, the down-regulated HCC cluster No. 13, which included many liver function-related genes, was also associated with AP1 [22,23]. Thus, in CH-B, the DNA damage response might trigger the signaling pathway of HCC, while AP1 in HCC is likely the key regulator of HBV-related HCC.

2.5. Framework of genetic clusters in relation to hepatocarcinogenesis of CH-C using GGM

In CH-C (Fig. 3B), the up-regulated non-cancerous cluster No. 1 correlated negatively with HCC cluster No. 9 and positively with HCC cluster No. 2. Non-cancerous cluster No. 1 was composed of interferon alpha/beta signaling pathway and leukocyte chemotaxis genes. HCC cluster No. 9 was composed of signal transduction and regulation of cell proliferation genes and associated directly with HCC cluster No. 18. HCC cluster Nos. 15 and 18 were composed of development process and wnt signaling pathway genes. HCC cluster Nos. 12 and 14 were composed of immune development, cell adhesion, and defense response genes. These clusters were directly and indirectly associated with HCC cluster No.9. HCC cluster No. 2 was composed of liver function genes, including those for lipid metabolism and iron ion transport. Non-cancerous cluster No. 7, which was composed of immune response, G-protein signaling, and regulation of lipid metabolism genes, correlated positively with HCC cluster No. 18.

Fig. 1. One way hierarchical clustering of 783 differentially expressed genes in CH-B-related HCC.A total of 783 genes were differentially expressed in CH-B-related HCC. Up-regulated genes are shown in red, down-regulated genes are shown in green, and unchanged genes are shown in white.

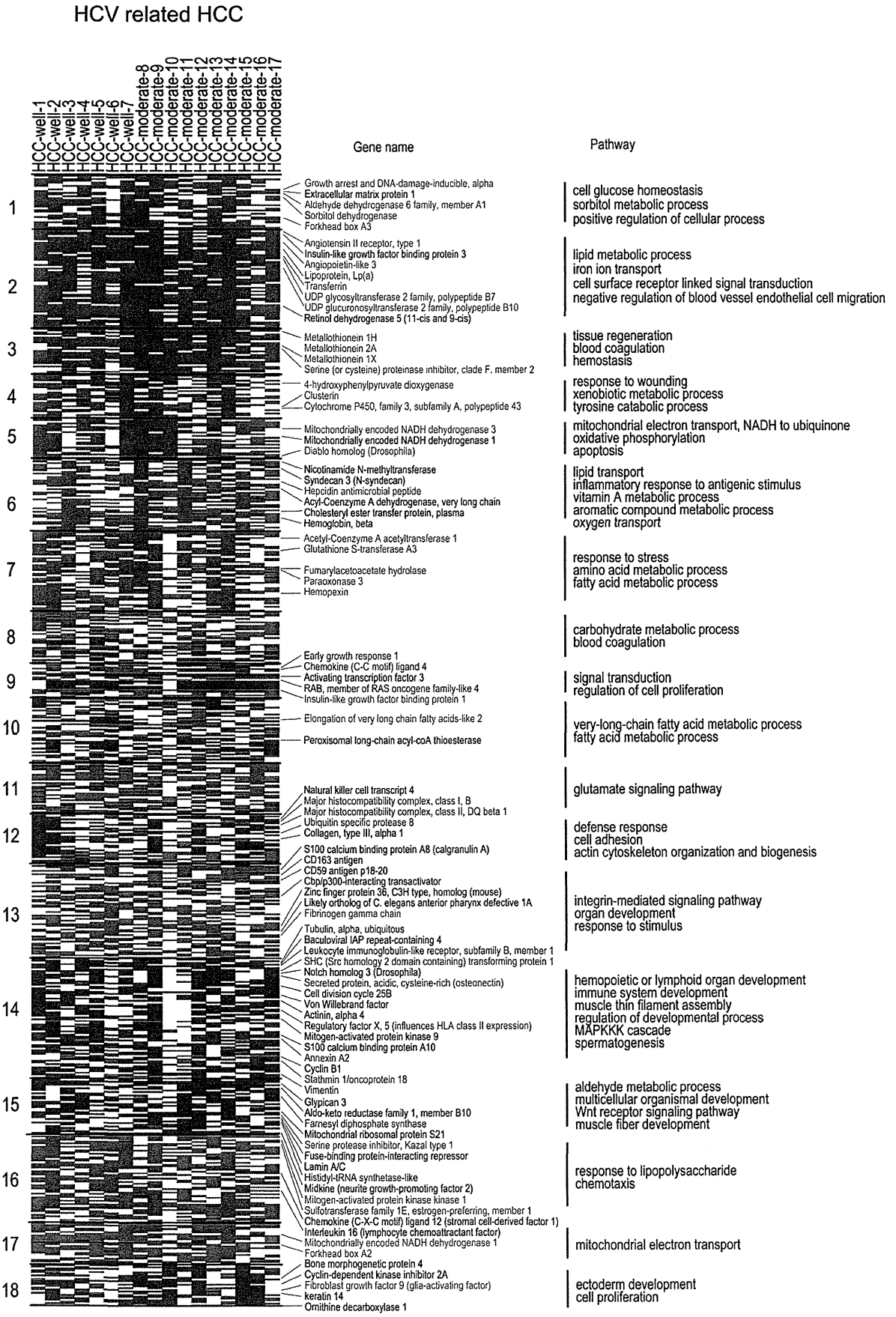
HCV related HCC
HCC-well-1
HCC-well-2
HCC-well-3
HCC-well-4
HCC-well-5
HCC-well-6
HCC-well-7
HCC-moderate-8
HCC-moderate-9
HCC-moderate-10
HCC-moderate-11
HCC-moderate-12
HCC-moderate-13
HCC-moderate-14
HCC-moderate-15
HCC-moderate-16
HCC-moderate-17
Gene name
Pathway
1
Growth arrest and DNA-damage-inducible, alpha
Extracellular matrix protein 1
Aldehyde dehydrogenase 6 family, member A1
Sorbitol dehydrogenase
Forkhead box A3
cell glucose homeostasis
sorbitol metabolic process
positive regulation of cellular process
2
Angiotensin II receptor, type 1
Insulin-like growth factor binding protein 3
Angiopoietin-like 3
Lipoprotein, Lp(a)
Transferrin
UDP glycosyltransferase 2 family, polypeptide B7
UDP glucuronosyltransferase 2 family, polypeptide B10
Retinol dehydrogenase 5 (11-cis and 9-cis)
lipid metabolic process
iron ion transport
cell surface receptor linked signal transduction
negative regulation of blood vessel endothelial cell migration
3
Metallothionein 1H
Metallothionein 2A
Metallothionein 1X
Serine (or cysteine) proteinase inhibitor, clade F, member 2
tissue regeneration
blood coagulation
hemostasis
4
4-hydroxyphenylpyruvate dioxygenase
Clusterin
Cytochrome P450, family 3, subfamily A, polypeptide 43
response to wounding
xenobiotic metabolic process
tyrosine catabolic process
5
Mitochondrially encoded NADH dehydrogenase 3
Mitochondrially encoded NADH dehydrogenase 1
Diablo homolog (Drosophila)
mitochondrial electron transport, NADH to ubiquinone
oxidative phosphorylation
apoptosis
6
Nicotinamide N-methyltransferase
Syndecan 3 (N-syndecan)
Hepcidin antimicrobial peptide
Acyl-Coenzyme A dehydrogenase, very long chain
Cholesteryl ester transfer protein, plasma
Hemoglobin, beta
lipid transport
inflammatory response to antigenic stimulus
vitamin A metabolic process
aromatic compound metabolic process
oxygen transport
7
Acetyl-Coenzyme A acetyltransferase 1
Glutathione S-transferase A3
Fumarylacetoacetate hydrolase
Paraoxonase 3
Hemopexin
response to stress
amino acid metabolic process
fatty acid metabolic process
8
carbohydrate metabolic process
blood coagulation
9
Early growth response 1
Chemokine (C-C motif) ligand 4
Activating transcription factor 3
RAB, member of RAS oncogene family-like 4
Insulin-like growth factor binding protein 1
signal transduction
regulation of cell proliferation
10
Elongation of very long chain fatty acids-like 2
Peroxisomal long-chain acyl-coA thioesterase
very-long-chain fatty acid metabolic process
fatty acid metabolic process
11
Natural killer cell transcript 4
glutamate signaling pathway
12
Major histocompatibility complex, class I, B
Major histocompatibility complex, class II, DQ beta 1
Ubiquitin specific protease 8
Collagen, type III, alpha 1
defense response
cell adhesion
13
S100 calcium binding protein A8 (calgranulin A)
CD163 antigen
CD59 antigen p18-20
Cbp/p300-interacting transactivator
Zinc finger protein 36, C3H type, homolog (mouse)
Likely ortholog of C. elegans anterior pharynx defective 1A
Fibrinogen gamma chain
Tubulin, alpha, ubiquitous
Baculoviral IAP repeat-containing 4
Leukocyte immunoglobulin-like receptor, subfamily B, member 1
SHC (Src homology 2 domain containing) transforming protein 1
actin cytoskeleton organization and biogenesis
integrin-mediated signaling pathway
organ development
response to stimulus
14
Notch homolog 3 (Drosophila)
Secreted protein, acidic, cysteine-rich (osteonectin)
Cell division cycle 25B
Von Willebrand factor
Actinin, alpha 4
Regulatory factor X, 5 (influences HLA class II expression)
Mitogen-activated protein kinase 9
S100 calcium binding protein A10
Annexin A2
Cyclin B1
hemopoietic or lymphoid organ development
immune system development
muscle thin filament assembly
regulation of developmental process
MAPKKK cascade
spermatogenesis
15
Stathmin 1/oncoprotein 18
Vimentin
Glypican 3
Aldo-keto reductase family 1, member B10
Farnesyl diphosphate synthase
Mitochondrial ribosomal protein S21
aldehyde metabolic process
multicellular organismal development
Wnt receptor signaling pathway
muscle fiber development
16
Serine protease inhibitor, Kazal type 1
Fuse-binding protein-interacting repressor
Lamin A/C
Histidyl-tRNA synthetase-like
Midkine (neurite growth-promoting factor 2)
Milogen-activated protein kinase kinase 1
Sulfotransferase family 1E, estrogen-preferring, member 1
Chemokine (C-X-C motif) ligand 12 (stromal cell-derived factor 1)
response to lipopolysaccharide
chemotaxis
17
Interleukin 16 (lymphocyte chemoattractant factor)
Mitochondrially encoded NADH dehydrogenase 1
Forkhead box A2
mitochondrial electron transport
18
Bone morphogenetic protein 4
Cyclin-dependent kinase inhibitor 2A
Fibroblast growth factor 9 (glia-activating factor)
keratin 14
Ornithine decarboxylase 1
ectoderm development
cell proliferation

Table 2
Characteristic genes expressed in CH-C-related HCC.

Genes	Symbol	GenBank ID	Cluster No.	Up- or down-regulated	GO
Acetyl-coenzyme A acetyltransferase 1	ACAT1	NM_000019	7	Down	Metabolic process
Chemokine (C-C motif) ligand 19	CCL19	NM_006274	12	Up	Immune response
Natural killer cell transcript 4 (Interleukin 32)	IL32	NM_004221	12	Up	Immune response
Major histocompatibility complex, class I, B	HLA-B	NM_005514	12	Up	Immune response
Major histocompatibility complex, class II, DQ beta 1	HLA-DQB1	NM_002123	12	Up	Immune response
Ubiquitin specific protease 8	USP8	NM_005154	12	Up	Cell proliferation
Tubulin, alpha 1b	TUBA1B	NM_006082	14	Up	Microtubule cytoskeleton organization
Actin, alpha 2	ACTA2	NM_001613	14	Up	Vascular smooth muscle contraction
SHC transforming protein 1	SHC1	NM_183001	14	Up	Activation of MAPK activity
Sterile alpha motif domain containing 9	SAMD9	NM_017654	14	Up	Regulation of transcription, dna-dependent
S100 calcium binding protein A10	*S100A10*	NM_002964	14	Up	Signal transduction
Annexin A2	ANXA2	NM_017654	14	Up	Skeletal system development
Cyclin B1	CCNB1	M25753	14	Up	Cell cycle
Platelet-activating factor acetylhydrolase 1b, 3	PAFAH1B3	D63391	14	Up	Spermatogenesis
Vimentin	VIM	NM_003380	14	Up	Cell motion
Glypican 3	GPC3	NM_004484	15	Up	Anatomical structure morphogenesis
Aldo-keto reductase family 1, member B10	AKR1B10	NM_020299	15	Up	Cellular aldehyde metabolic process
ATP citrate lyase	ACLY	AI819617	15	Up	Lipid biosynthetic process
Farnesyl diphosphate synthase	FDPS	NM_002004	15	Up	Cholesterol biosynthetic process
Serine protease inhibitor, Kazal type 1	SPINK1	NM_003122	15	Up	Protein binding
Bone morphogenetic protein 4	BMP4	D30751	18	Up	Germ cell development
Cyclin-dependent kinase inhibitor 2A	CDKN2A	L27211	18	Up	Cell cycle checkpoint
Fibroblast growth factor 9	FGF9	D14838	18	Up	Signal transduction
Ornithine decarboxylase 1	ODC1	NM_002539	18	Up	Positive regulation of cell proliferation

Analysis of the individual gene interactions (Fig. 4B) showed that a key regulator gene of non-cancerous cluster No. 1, signal transducer and activator of transcription 1 (STAT1), negatively regulated early growth response protein 1 (EGR1) in HCC cluster No. 9 [24]. EGR1 was a key regulator of angiogenesis and fibrogenesis-inducing genes, such as PAI-1 (No. 9), COL1A1, and FAK1 (No. 18) [25–27]. In addition, EGR1 negatively regulated a key regulator of gluconeogenesis, PEPCK (No. 2) [28]. Thus, EGR1 regulated the tissue repair response as well as the metabolic process. In addition to STAT1, phosphatase and tensin homolog (PTEN), in non-cancerous cluster No. 7, negatively regulated FAK1 in HCC cluster No. 18 [29]. FAK1 regulated oncogene SHC (No. 14) and might be involved in the cancer signaling pathway [30,31]. Interestingly, PTEN was associated with Oct-3/4, a regulator of liver differentiation through its target gene C/EBP alpha (No. 3); C/EBP alpha regulated CYP27A1 and CYP3A5 (No. 5). Thus, in CH-C, two antitumor genes, STAT1 and PTEN, were associated with the expression of EGR1 and FAK1, which promote angiogenesis, fibrogenesis, and tumorigenesis in cancerous lesions. Interestingly, the expression of PTEN was related to the metabolic process of CH-C.

2.6. Serial gene expression in non-cancerous gene clusters and the occurrence of HCC

Analysis of the framework of gene clusters in relation to hepatocarcinogenesis by GGM and individual gene interactions revealed several key genes that were associated with hepatocarcinogenesis in non-cancerous clusters. We focused on STAT1 and PTEN in non-cancerous clusters in CH-C and evaluated serial changes of their expression at 2 time points (tumor free and tumor present) in additional 11 patients. The clinical characteristics of these patients at both time points are shown in Supplemental Table J. The expression of STAT1 and its related genes significantly decreased at the time of HCC development compared with the tumor-free time. Similarly, the expression of PTEN significantly decreased when HCC developed compared with the tumor-free time (Supplemental Fig. C2, 3).

3. Discussion

HCC frequently develops in the advanced stage of liver fibrosis. Although gene expression profiling of HCC and the background liver has been studied extensively [32–35], the relationship between the gene expression profiles of different lesions has not been elucidated. In the present study, we utilized GGM [15,16] to analyze the relationship between gene expression in HCC and non-cancerous liver. GGM is widely utilized to study gene association networks [12–14].

We first performed gene expression profiling in CH-B- and CH-C-related HCC. The up- and down-regulated genes were identified by a comparison with a single reference sample of normal liver. There may be some variations in gene expression among normal livers; however, the identified genes were characteristic of HCC and were consistent with previous reports [33,34]. Differences in the signaling pathways between CH-B- and CH-C-related HCC are clearly shown in Figs. 1 and 2 and Supplemental Fig. D. In CH-C-related HCC, immune response- and cytoskeleton-related genes, such as actin, tubulin, and vimentin, were up-regulated, while in CH-B-related HCC, cell matrix interaction genes, such as collagen IV and matrix metalloproteinase, were up-regulated. HBV-X protein reportedly promotes HCC metastasis by the up-regulation of matrix metalloproteinases [36]. The differences in the gene expression profiles between CH-C- and CH-B-related HCC were concordant with those reported previously [34,37].

In the present study, GGM analysis also revealed the interactions of each cluster within HCC as well as within non-cancerous lesions. GGM analysis in CH-B-related HCC showed that 3 up-regulated clusters and 6 down-regulated clusters were associated with each other. In CH-C-related HCC, 4 up-regulated gene clusters and 5 down-regulated gene clusters were associated with each other (Fig. 3). Interestingly, the up-regulated gene clusters were preferentially expressed in CPA in the liver. This prompted us to consider the origin of the HCC cells. Recent reports of immunohistochemical staining of liver tissue using stem cell markers, such as EpCAM and CD133, have suggested the presence of hepatic stem cells in the periportal area [38]. In contrast, many of the down-regulated genes were liver function and metabolism-related genes that were preferentially expressed in CLL in the liver.

Fig. 2. One way hierarchical clustering of 668 differentially expressed genes in CH-B-related HCC.A total of 668 genes were differentially expressed in CH-C-related HCC. Up-regulated genes are shown in red, down-regulated genes are shown in green, and unchanged genes are shown in white (Fig. 2).

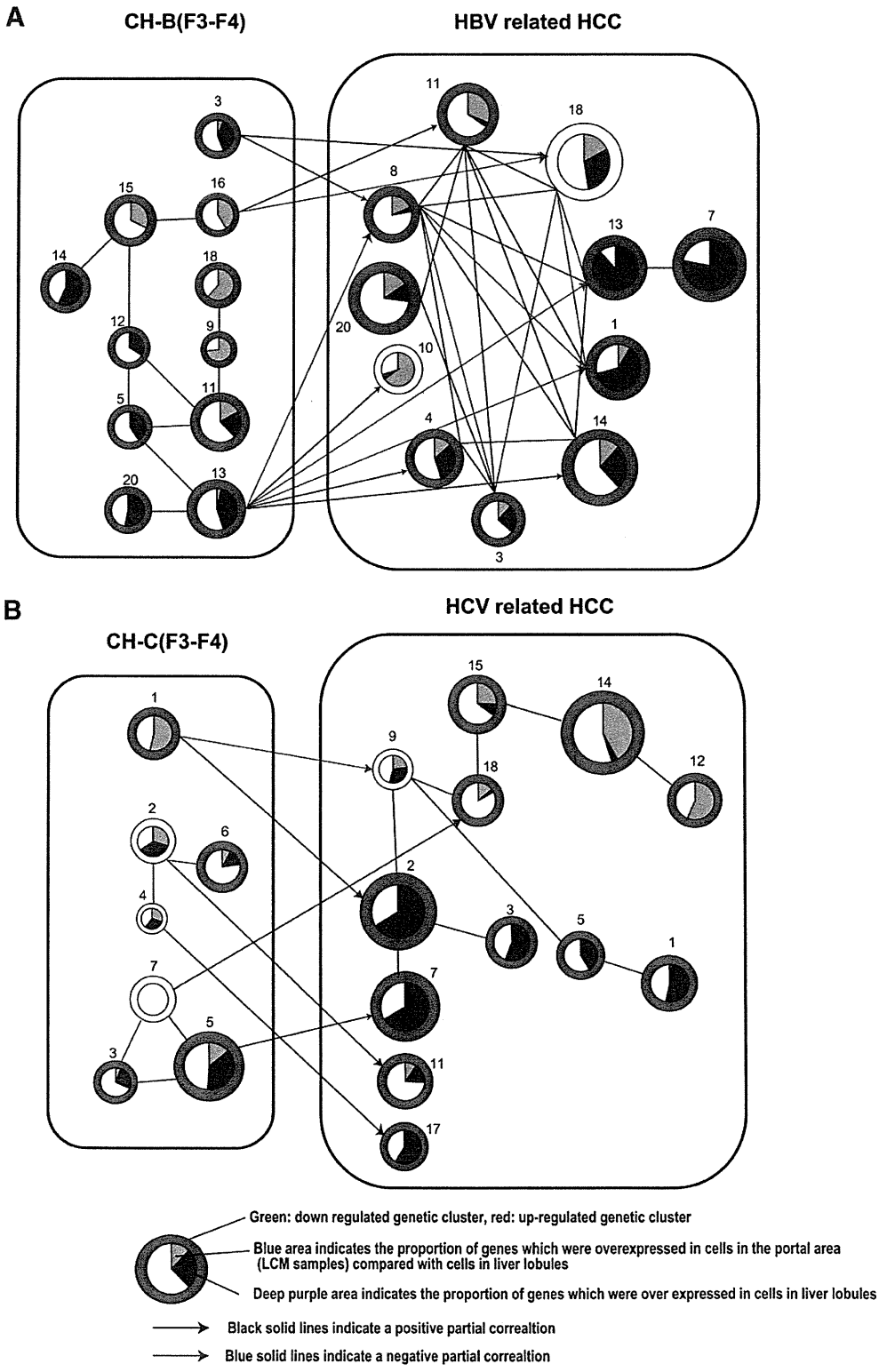

Fig. 3. GGM analysis of each cluster in HCC and non-cancerous lesions. Each cluster in the HCC and non-cancerous lesions was connected according to partial correlation coefficient matrix (PCCM) by GGM algorithms (Supplemental Tables H and I). The blue lines indicate a negative partial correlation and the black lines indicate a positive partial correlation. The size of each cluster reflects the number of clustered genes. The red circles are up-regulated gene clusters, while the green circles are down-regulated gene clusters. Within each cluster, the blue area indicates the proportion of genes that are over-expressed in CPA, while the deep purple area indicates the proportion of genes that are over-expressed in CLL. A; interactions of HBV related clusters. B; interactions of HCV related clusters.

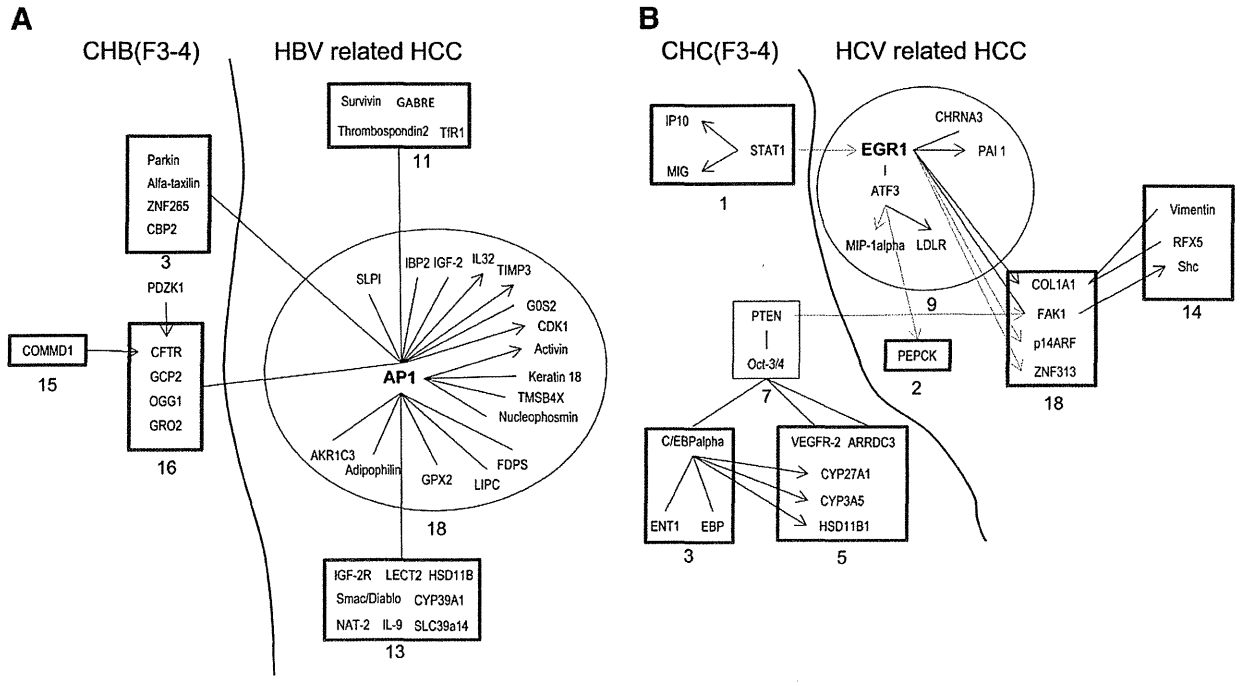

Fig. 4. Individual gene interactions between gene clusters in HCC and non-cancerous lesions. Direct interactions of individual genes among each cluster were confirmed by reference to the MetaCore database. The blue arrows indicate negative regulation, while the black arrows indicate positive regulation. Unspecified interactions are shown with black lines. The red squares are up-regulated gene clusters, while the green squares are down-regulated gene clusters. A; direct interactions of genes in HBV related clusters. B; direct interactions of genes in HCV related clusters.

GGM analysis between the HCC and non-cancerous liver revealed the unique interactions of 2 lesions in this study. In CH-B, up-regulated cluster Nos. 3 and 16, development and DNA damage response gene clusters, regulated HCC cluster Nos. 8, 11, and 18, VEGF-family signaling, apoptosis and survival-related, and ESR1 regulation of G1/S transition-related gene clusters. Down-regulated cluster No. 13, a metabolism-related gene cluster, negatively regulated the up-regulated HCC cluster No. 8. These results suggest that the metabolic status of non-cancerous liver influences the gene expression of HCC. Individual gene interactions with reference to the MetaCore database showed that 8 genes in non-cancerous cluster Nos. 3 and 16 were directly associated with AP1 in HCC cluster No. 18, which regulated the expression of many HCC genes (Fig. 4) [18–23]. Interestingly, the HBV transcript was clustered in HCC cluster No. 18. It has been reported that the HBV transcript enhances AP-1 activation [39,40]. The results suggest a role for the HBV transcript in CH-B-related HCC. Recently, a next generation sequencing approach revealed the frequent integration of HBV in HCC (86.4%), where the putative cancer-related human telomerase reverse transcriptase (hTERT), mixed-lineage leukemia 4, and cyclin E1 genes were located [41]. Although, we could not find the up-regulation of these genes in CH-B-related HCC, HBV genome integration should have important roles for HBV-related hepatocarcinogenesis. A previous report demonstrated that HBx retained the ability to overcome active oncogene RAS-induced senescence by using hTERT, which was introduced into human immortalized primary cells [42].

In CH-C, STAT1 and PTEN signaling in cluster Nos. 1 and 7, respectively, were associated with HCC cluster Nos. 9, 18, and 2, EGR1 signaling, ectodermal development and cell proliferation, lipid metabolism, and iron transport gene clusters. Individual gene interactions with reference to the MetaCore database showed that EGR1 regulates multiple genes in HCC cluster No. 9 as well as genes in up-regulated HCC cluster No. 18 and down-regulated HCC cluster No. 2 (Fig. 4). STAT1 and PTEN in non-cancerous cluster Nos. 1 and 7 exhibited an anti-tumor effect.

STAT1 negatively regulated EGR1 [24] and, interestingly, the expression of PTEN was associated with metabolic-related genes in non-cancerous cluster Nos. 3 and 5 (Fig. 4). PTEN reportedly promotes oxidative phosphorylation, decreases glycolysis, and prevents the metabolic reprogramming of cancer cells [43].

The reduced expression of these antitumor genes in CH-C might increase the expression of EGR1 and FAK1, which promote angiogenesis, fibrogenesis, and tumorigenesis in HCC (Fig. 4). EGR-1 promotes hepatocellular mitotic progression [44], while p53 and PTEN are downstream targets of EGR1. EGR1 might be involved in a negative feedback mechanism of cell cycle progression by inducing p53 and PTEN [45]. Recent reports described the tumorigenic role of EGR1 in the presence of p53 and PTEN mutations [46,47]. Thus, interferon signaling evoked by an innate immune response and the PTEN expression-associated metabolic process (Nos. 3 and 5) will likely regulate the gene expression profile of HCC through EGR1.

It is reported that HBV X protein represses the expression of PTEN by inhibiting the function of p53 [48] and c-Jun promotes cellular survival by suppression of PTEN [49]. In this study, the expression of PTEN was repressed in CH-B (Supplemental Fig. B, CH-B, cluster 21). Possible involvement of HBx, AP-1 and PTEN signaling in HBV-related hepatocarcinogenesis should be explored furthermore.

Recently, Hoshida et al. reported that gene expression profiling of the background liver of patients with HCC predicts their outcome [35]. In their report, gene sets, which correlated with good survival, included many metabolic process genes, such as those of fatty acid, amino acid, and glucose metabolism. In accordance with their results, our findings showed that the possible involvement of metabolic process genes in the background liver might influence gene expression in HCC. In addition, our study revealed the predisposing changes of gene expression in non-cancerous liver that precede the changes of gene expression in HCC. Interestingly, we found that the expression of the anti-tumor genes STAT1 and PTEN was decreased significantly at the onset of HCC compared with the tumor-free time. Therefore, serial analysis of the expression of these genes might be useful for predicting the development of HCC. Several reports have shown that the decreased expression of some chemokines, such as CXCL10, CCL2, and CCL5, is associated with the poor prognosis of resectable HCC [50,51]. In this study, the expression of CXCL10, CXCL6, CXCL9,

and macrophage migration inhibitory factor was decreased at the onset of HCC compared with the tumor-free time (Supplemental Fig. C). It would be worthwhile to examine the expression of these genes in serum samples to predict the development of HCC.

In summary, using a bioinformatics approach, we performed gene expression profiling of HCC and non-cancerous liver, which revealed the predisposing changes of gene expression in HCC. This approach will be useful for the early diagnosis of HCC. Further studies with a larger sample population are needed to confirm our data and to determine possible means for preventing the development of HCC.

4. Materials and methods

4.1. Patients and tissue samples

HCC and non-cancerous liver specimens were obtained from 17 patients with HCV-related HCC and 17 with HBV-related HCC who underwent surgical resection of the liver (Supplemental Tables A and B). For the control normal liver, a surgically obtained tissue sample from a patient who showed no clinical signs of hepatitis was used as described previously [9,10]. The liver tissue was histologically normal, and the patient tested negative for all hepatitis virus markers and had normal levels of serum aminotransferase. HCC and non-cancerous liver tissues were enucleated from resected specimens and frozen immediately in liquid nitrogen for RNA isolation [10]. In a previous study, expression profiling of the liver of 19 patients with CH-B and 18 with CH-C was performed (Table 2) [10]. The other experimental procedures are described in the Supplemental Materials and Methods.

4.2. Microarray analysis

cDNA microarray slides (Liver chip 10 k) were used as described previously [10]. For the selection of genes, we utilized data from the cDNA microarray and hepatic SAGE libraries derived from normal liver, CH-C, CH-C-related HCC, CH-B, and CH-B-related HCC, including 52,149 unique tags. We selected 9614 non-redundant genes that are expressed in diseased and normal liver. The detailed procedures for the preparation of the cDNA microarray slides are described in the Supplemental Material and Methods. RNA isolation, amplification of antisense RNA, labeling, and hybridization were performed according to the protocols described previously [10]. Quantitative assessment of the signals on the slides was performed by scanning on a ScanArray 5000 (General Scanning, Watertown, MA) followed by image analysis using GenePix Pro 4.1 (Axon Instruments, Union City, CA) as described previously [10]. The microarray data have been submitted to the Gene Expression Omnibus (GEO) public database at NCBI (Accession No. GSE41804). The details are also described in the Supplemental Material and Methods.

4.3. Graphical Gaussian modeling data processing

GGM [15,16] enabled us to reveal the gene cluster framework in relation to hepatocellular carcinogenesis of CH-B and CH-C. The procedure included: 1) gene clustering; 2) construction of the PCCM by GGM algorithms; and 3) visualization of the cluster pathway (Supplemental Fig. A).

4.4. Gene selection

To utilize a variety of tissue samples, we first calculated the ratio of gene expression in non-cancerous tissue (36 with CH-B and 35 with CH-C) to that in normal tissue and the ratio of gene expression in HCC tissue (17 with CH-B related HCC and 17 with CH-C related HCC) to that in normal tissue. Then, the expression ratios of non-cancerous and HCC tissues in individual samples were standardized in the two tissues, respectively, by transformation to the Z score (each value was subtracted by the average value and divided by the standard deviation (SD)) such that the mean expression value was 0 and the SD was 1. A gene was regarded as differentially expressed if the Z score was >1 or <-1 ($1 > |AV \pm SD|$). Although the criterion for a differentially expressed gene is usually $|AV \pm 2SD|$, the selection procedure described above is simply designed to gather as many differentially expressed genes as possible, and is suitable for determining the macroscopic relationships between gene systems estimated by cluster analysis. Gene selection from non-HCC samples was performed similarly by avoiding the selected genes in HCC (backward selection). Therefore, a correlation between HCC and non-HCC genes could be obtained as there was no overlap between the genes.

4.5. Clustering with automatic determination of cluster number

In gene profile clustering, the Euclidian distance between Pearson's correlation coefficient of profiles and the unweighted pair group method using the arithmetic average (UPGMA or group average method) were adopted as the metric and the technique, respectively, with reference to previous GGM analysis [15,16]. Note that the present metric and technique were selected to estimate robustly the clusters against the noise of gene expression measurements [15]. In cluster number estimation, the variance inflation factor was adopted as a stopping rule for the hierarchical clustering of expression profiles [15], and the popular cutoff value of 10.0 [52] was adopted as the threshold.

4.6. Graphical Gaussian modeling

The average expression profiles were calculated for the members of each cluster, and the average correlation coefficient matrix between the clusters was calculated. The average correlation coefficient matrix between the clusters was then subjected to GGM as described previously [15,16]. The correlation coefficient can return a false value in the presence of confounding factors. Partial correlation enables replacement of a false-positive correlation with the actual correlation. The PCCM was calculated using GGM (Supplemental Fig. A). All calculations for clustering analysis and GGM were performed via the ASIAN web site (http://eureka.cbrc.jp/asian/index_j.html) [53] and "Auto Net Finder," a commercial desktop version of ASIAN (Infocom Corporation, Shibuya, Tokyo, Japan, http://www.infocom.co.jp/bio/download/).

4.7. Rearrangement of the inferred network

Since the magnitude of the partial correlation coefficient indicates the strength of the association between clusters, the intact network can be rearranged according to the partial correlation coefficient to interpret the association between clusters. The strength of the association can be assigned by a standard test for the partial correlation coefficient. In the present study, the significance level in the *t*-test was 1% (Supplemental Fig. A).

4.8. Gene ontology of cluster members

Functional ontology enrichment analysis was performed to examine the gene ontology process distribution of each cluster gene using MetaCore™ (Thomson Reuters, New York, NY). Gene ontology was also confirmed by DAVID Bioinformatics Resources 6.7 (http://david.abcc.ncifcrf.gov/) [17].

Supplementary data to this article can be found online at http://dx.doi.org/10.1016/j.ygeno.2013.02.007.

Acknowledgments

The authors thank Nami Nishiyama for excellent technical assistance.

References

[1] R. Siegel, D. Naishadham, A. Jemal, Cancer statistics, 2012, CA Cancer J. Clin. 62 (2012) 10–29.
[2] H. Tsukuma, T. Hiyama, S. Tanaka, M. Nakao, T. Yabuuchi, T. Kitamura, K. Nakanishi, I. Fujimoto, A. Inoue, H. Yamazaki, Risk factors for hepatocellular carcinoma among patients with chronic liver disease, N. Engl. J. Med. 328 (1993) 1797–1801.
[3] A. Arzumanyan, H.M. Reis, M.A. Feitelson, Pathogenic mechanisms in HBV- and HCV-associated hepatocellular carcinoma, Nat. Rev. Cancer 13 (2012) 123–135.
[4] H. Yoshida, Y. Shiratori, M. Moriyama, Y. Arakawa, T. Ide, M. Sata, O. Inoue, M. Yano, M. Tanaka, S. Fujiyama, S. Nishiguchi, T. Kuroki, F. Imazeki, O. Yokosuka, S. Kinoyama, G. Yamada, M. Omata, Interferon therapy reduces the risk for hepatocellular carcinoma: national surveillance program of cirrhotic and noncirrhotic patients with chronic hepatitis C in Japan. IHIT Study Group. Inhibition of hepatocarcinogenesis by interferon therapy, Ann. Intern. Med. 131 (1999) 174–181.
[5] G. Fattovich, T. Stroffolini, I. Zagni, F. Donato, Hepatocellular carcinoma in cirrhosis: incidence and risk factors, Gastroenterology 127 (2004) S35–S50.
[6] A. de La Coste, B. Romagnolo, P. Billuart, C.A. Renard, M.A. Buendia, O. Soubrane, M. Fabre, J. Chelly, C. Beldjord, A. Kahn, C. Perret, Somatic mutations of the beta-catenin gene are frequent in mouse and human hepatocellular carcinomas, Proc. Natl. Acad. Sci. U. S. A. 95 (1998) 8847–8851.
[7] D.F. Calvisi, S. Ladu, A. Gorden, M. Farina, E.A. Conner, J.S. Lee, V.M. Factor, S.S. Thorgeirsson, Ubiquitous activation of Ras and Jak/Stat pathways in human HCC, Gastroenterology 130 (2006) 1117–1128.
[8] G.H. Thoresen, T.K. Guren, D. Sandnes, M. Peak, L. Agius, T. Christoffersen, Response to transforming growth factor alpha (TGFalpha) and epidermal growth factor (EGF) in hepatocytes: lower EGF receptor affinity of TGFalpha is associated with more sustained activation of p42/p44 mitogen-activated protein kinase and greater efficacy in stimulation of DNA synthesis, J. Cell. Physiol. 175 (1998) 10–18.
[9] M. Honda, S. Kaneko, H. Kawai, Y. Shirota, K. Kobayashi, Differential gene expression between chronic hepatitis B and C hepatic lesion, Gastroenterology 120 (2001) 955–966.
[10] M. Honda, T. Yamashita, T. Ueda, H. Takatori, R. Nishino, S. Kaneko, Different signaling pathways in the livers of patients with chronic hepatitis B or chronic hepatitis C, Hepatology 44 (2006) 1122–1138.
[11] M. Honda, M. Nakamura, M. Tateno, A. Sakai, T. Shimakami, T. Shirasaki, T. Yamashita, K. Arai, T. Yamashita, Y. Sakai, S. Kaneko, Differential interferon signaling in liver lobule and portal area cells under treatment for chronic hepatitis C, J. Hepatol. 53 (2010) 817–826.
[12] H. Kishino, P.J. Waddell, Correspondence analysis of genes and tissue types and finding genetic links from microarray data, Genome Inform. Ser. Workshop Genome Inform. 11 (2000) 83–95.
[13] P.J. Waddell, H. Kishino, Cluster inference methods and graphical models evaluated on NCI60 microarray gene expression data, Genome Inform. Ser. Workshop Genome Inform. 11 (2000) 129–140.
[14] J. Krumsiek, K. Suhre, T. Illig, J. Adamski, F.J. Theis, Gaussian graphical modeling reconstructs pathway reactions from high-throughput metabolomics data, BMC Syst. Biol. 5 (2011) 21.
[15] H. Toh, K. Horimoto, Inference of a genetic network by a combined approach of cluster analysis and graphical Gaussian modeling, Bioinformatics 18 (2002) 287–297.
[16] S. Aburatani, F. Sun, S. Saito, M. Honda, S. Kaneko, K. Horimoto, Gene systems network inferred from expression profiles in hepatocellular carcinogenesis by graphical Gaussian model, EURASIP J. Bioinform. Syst. Biol. (2007) 47214.
[17] W. Huang da, B.T. Sherman, Q. Tan, J. Kir, D. Liu, D. Bryant, Y. Guo, R. Stephens, M.W. Baseler, H.C. Lane, R.A. Lempicki, DAVID bioinformatics resources: expanded annotation database and novel algorithms to better extract biology from large gene lists, Nucleic Acids Res. 35 (2007) W169–W175.
[18] L. Russell, D.R. Forsdyke, A human putative lymphocyte G0/G1 switch gene containing a CpG-rich island encodes a small basic protein with the potential to be phosphorylated, DNA Cell Biol. 10 (1991) 581–591.
[19] L. Zhong, J. Ou, U. Barkai, J.F. Mao, J. Frasor, G. Gibori, Molecular cloning and characterization of the rat ovarian 20 alpha-hydroxysteroid dehydrogenase gene, Biochem. Biophys. Res. Commun. 249 (1998) 797–803.
[20] K.M. Mani, C. Lefebvre, K. Wang, W.K. Lim, K. Basso, R. Dalla-Favera, A. Califano, A systems biology approach to prediction of oncogenes and molecular perturbation targets in B-cell lymphomas, Mol. Syst. Biol. 4 (2008) 169.
[21] H.K. Kwon, J.S. Hwang, J.S. So, C.G. Lee, A. Sahoo, J.H. Ryu, W.K. Jeon, B.S. Ko, C.R. Im, S.H. Lee, Z.Y. Park, S.H. Im, Cinnamon extract induces tumor cell death through inhibition of NFkappaB and AP1, BMC Cancer 10 (2010) 392.
[22] K.R. Mitchell, D. Warshawsky, Xenobiotic inducible regions of the human arylamine N-acetyltransferase 1 and 2 genes, Toxicol. Lett. 139 (2003) 11–23.
[23] D. Bottomly, S.L. Kyler, S.K. McWeeney, G.S. Yochum, Identification of {beta}-catenin binding regions in colon cancer cells using ChIP-Seq, Nucleic Acids Res. 38 (2010) 5735–5745.
[24] J.L. Ingram, A. Antao-Menezes, J.B. Mangum, O. Lyght, P.J. Lee, J.A. Elias, J.C. Bonner, Opposing actions of Stat1 and Stat6 on IL-13-induced up-regulation of early growth response-1 and platelet-derived growth factor ligands in pulmonary fibroblasts, J. Immunol. 177 (2006) 4141–4148.
[25] H. Liao, M.C. Hyman, D.A. Lawrence, D.J. Pinsky, Molecular regulation of the PAI-1 gene by hypoxia: contributions of Egr-1, HIF-1alpha, and C/EBPalpha, FASEB J. 21 (2007) 935–949.
[26] V. Lejard, F. Blais, M.J. Guerquin, A. Bonnet, M.A. Bonnin, E. Havis, M. Malbouyres, C.B. Bidaud, G. Maro, P. Gilardi-Hebenstreit, J. Rossert, F. Ruggiero, D. Duprez, EGR1 and EGR2 involvement in vertebrate tendon differentiation, J. Biol. Chem. 286 (2011) 5855–5867.
[27] V. Golubovskaya, A. Kaur, W. Cance, Cloning and characterization of the promoter region of human focal adhesion kinase gene: nuclear factor kappa B and p53 binding sites, Biochim. Biophys. Acta 1678 (2004) 111–125.
[28] S.P. Berasi, C. Huard, D. Li, H.H. Shih, Y. Sun, W. Zhong, J.E. Paulsen, E.L. Brown, R.E. Gimeno, R.V. Martinez, Inhibition of gluconeogenesis through transcriptional activation of EGR1 and DUSP4 by AMP-activated kinase, J. Biol. Chem. 281 (2006) 27167–27177.
[29] J. Gu, M. Tamura, R. Pankov, E.H. Danen, T. Takino, K. Matsumoto, K.M. Yamada, Shc and FAK differentially regulate cell motility and directionality modulated by PTEN, J. Cell Biol. 146 (1999) 389–403.
[30] J.F. Rual, K. Venkatesan, T. Hao, T. Hirozane-Kishikawa, A. Dricot, N. Li, G.F. Berriz, F.D. Gibbons, M. Dreze, N. Ayivi-Guedehoussou, N. Klitgord, C. Simon, M. Boxem, S. Milstein, J. Rosenberg, D.S. Goldberg, L.V. Zhang, S.L. Wong, G. Franklin, S. Li, J.S. Albala, J. Lim, C. Fraughton, E. Llamosas, S. Cevik, C. Bex, P. Lamesch, R.S. Sikorski, J. Vandenhaute, H.Y. Zoghbi, A. Smolyar, S. Bosak, R. Sequerra, L. Doucette-Stamm, M.E. Cusick, D.E. Hill, F.P. Roth, M. Vidal, Towards a proteome-scale map of the human protein–protein interaction network, Nature 437 (2005) 1173–1178.
[31] T.P. Hecker, J.R. Grammer, G.Y. Gillespie, J. Stewart, C.L. Gladson, Focal adhesion kinase enhances signaling through the Shc/extracellular signal-regulated kinase pathway in anaplastic astrocytoma tumor biopsy samples, Cancer Res. 62 (2002) 2699–2707.
[32] H. Okabe, S. Satoh, T. Kato, O. Kitahara, R. Yanagawa, Y. Yamaoka, T. Tsunoda, Y. Furukawa, Y. Nakamura, Genome-wide analysis of gene expression in human hepatocellular carcinomas using cDNA microarray: identification of genes involved in viral carcinogenesis and tumor progression, Cancer Res. 61 (2001) 2129–2137.
[33] Y. Hippo, K. Watanabe, A. Watanabe, Y. Midorikawa, S. Yamamoto, S. Ihara, S. Tokita, H. Iwanari, Y. Ito, K. Nakano, J. Nezu, H. Tsunoda, T. Yoshino, I. Ohizumi, M. Tsuchiya, S. Ohnishi, M. Makuuchi, T. Hamakubo, T. Kodama, H. Aburatani, Identification of soluble NH2-terminal fragment of glypican-3 as a serological marker for early-stage hepatocellular carcinoma, Cancer Res. 64 (2004) 2418–2423.
[34] Y. Shirota, S. Kaneko, M. Honda, H.F. Kawai, K. Kobayashi, Identification of differentially expressed genes in hepatocellular carcinoma with cDNA microarrays, Hepatology 33 (2001) 832–840.
[35] Y. Hoshida, A. Villanueva, M. Kobayashi, J. Peix, D.Y. Chiang, A. Camargo, S. Gupta, J. Moore, M.J. Wrobel, J. Lerner, M. Reich, J.A. Chan, J.N. Glickman, K. Ikeda, M. Hashimoto, G. Watanabe, M.G. Daidone, S. Roayaie, M. Schwartz, S. Thung, H.B. Salvesen, S. Gabriel, V. Mazzaferro, J. Bruix, S.L. Friedman, H. Kumada, J.M. Llovet, T.R. Golub, Gene expression in fixed tissues and outcome in hepatocellular carcinoma, N. Engl. J. Med. 359 (2008) 1995–2004.
[36] L. Xia, W. Huang, D. Tian, H. Zhu, Y. Zhang, H. Hu, D. Fan, Y. Nie, K. Wu, Upregulated FoxM1 expression induced by hepatitis B virus X protein promotes tumor metastasis and indicates poor prognosis in hepatitis B virus-related hepatocellular carcinoma, J. Hepatol. 57 (2012) 600–612.
[37] S. Ura, M. Honda, T. Yamashita, T. Ueda, H. Takatori, R. Nishino, H. Sunakozaka, Y. Sakai, K. Horimoto, S. Kaneko, Differential microRNA expression between hepatitis B and hepatitis C leading disease progression to hepatocellular carcinoma, Hepatology 49 (2009) 1098–1112.
[38] R. Turner, O. Lozoya, Y. Wang, V. Cardinale, E. Gaudio, G. Alpini, G. Mendel, E. Wauthier, C. Barbier, D. Alvaro, L.M. Reid, Human hepatic stem cell and maturational liver lineage biology, Hepatology 53 (2011) 1035–1045.
[39] K.M. Sze, G.K. Chu, J.M. Lee, I.O. Ng, C-terminal truncated HBx is associated with metastasis and enhances invasiveness via C-Jun / MMP10 activation in hepatocellular carcinoma, Hepatology (2012).
[40] Y. Tanaka, F. Kanai, T. Ichimura, K. Tateishi, Y. Asaoka, B. Guleng, A. Jazag, M. Ohta, J. Imamura, T. Ikenoue, H. Ijichi, T. Kawabe, T. Isobe, M. Omata, The hepatitis B virus X protein enhances AP-1 activation through interaction with Jab1, Oncogene 25 (2006) 633–642.
[41] W.K. Sung, H. Zheng, S. Li, R. Chen, X. Liu, Y. Li, N.P. Lee, W.H. Lee, P.N. Ariyaratne, C. Tennakoon, F.H. Mulawadi, K.F. Wong, A.M. Liu, R.T. Poon, S.T. Fan, K.L. Chan, Z. Gong, Y. Hu, Z. Lin, G. Wang, Q. Zhang, T.D. Barber, W.C. Chou, A. Aggarwal, K. Hao, W. Zhou, C. Zhang, J. Hardwick, C. Buser, J. Xu, Z. Kan, H. Dai, M. Mao, C. Reinhard, J. Wang, J.M. Luk, Genome-wide survey of recurrent HBV integration in hepatocellular carcinoma, Nat. Genet. 44 (2012) 765–769.
[42] N. Oishi, K. Shilagardi, Y. Nakamoto, M. Honda, S. Kaneko, S. Murakami, Hepatitis B virus X protein overcomes oncogenic RAS-induced senescence in human immortalized cells, Cancer Sci. 98 (2007) 1540–1548.
[43] A. Ortega-Molina, M. Serrano, PTEN in cancer, metabolism, and aging, Trends Endocrinol. Metab. (2012).
[44] Y. Liao, O.N. Shikapwashya, E. Shteyer, B.K. Dieckgraefe, P.W. Hruz, D.A. Rudnick, Delayed hepatocellular mitotic progression and impaired liver regeneration in early growth response-1-deficient mice, J. Biol. Chem. 279 (2004) 43107–43116.
[45] Y. Zwang, A. Sas-Chen, Y. Drier, T. Shay, R. Avraham, M. Lauriola, E. Shema, E. Lidor-Nili, J. Jacob-Hirsch, N. Amariglio, Y. Lu, G.B. Mills, G. Rechavi, M. Oren, E. Domany, Y. Yarden, Two phases of mitogenic signaling unveil roles for p53 and EGR1 in elimination of inconsistent growth signals, Mol. Cell 42 (2011) 524–535.
[46] J. Yu, S.S. Zhang, K. Saito, S. Williams, Y. Arimura, Y. Ma, Y. Ke, V. Baron, D. Mercola, G.S. Feng, E. Adamson, T. Mustelin, PTEN regulation by Akt-EGR1-ARF-PTEN axis, EMBO J. 28 (2009) 21–33.
[47] D. Lu, C. Han, T. Wu, Microsomal prostaglandin E synthase-1 promotes hepatocarcinogenesis through activation of a novel EGR1/beta-catenin signaling axis, Oncogene 31 (2012) 842–857.
[48] T.W. Chung, Y.C. Lee, J.H. Ko, C.H. Kim, Hepatitis B Virus X protein modulates the expression of PTEN by inhibiting the function of p53, a transcriptional activator in liver cells, Cancer Res. 63 (2003) 3453–3458.
[49] K. Hettinger, F. Vikhanskaya, M.K. Poh, M.K. Lee, I. de Belle, J.T. Zhang, S.A. Reddy, K. Sabapathy, c-Jun promotes cellular survival by suppression of PTEN, Cell Death Differ. 14 (2007) 218–229.

[50] V. Chew, C. Tow, M. Teo, H.L. Wong, J. Chan, A. Gehring, M. Loh, A. Bolze, R. Quek, V.K. Lee, K.H. Lee, J.P. Abastado, H.C. Toh, A. Nardin, Inflammatory tumour microenvironment is associated with superior survival in hepatocellular carcinoma patients, J. Hepatol. 52 (2010) 370–379.
[51] V. Chew, J. Chen, D. Lee, E. Loh, J. Lee, K.H. Lim, A. Weber, K. Slankamenac, R.T. Poon, H. Yang, L.L. Ooi, H.C. Toh, M. Heikenwalder, I.O. Ng, A. Nardin, J.P. Abastado, Chemokine-driven lymphocyte infiltration: an early intratumoural event determining long-term survival in resectable hepatocellular carcinoma, Gut 61 (2012) 427–438.
[52] R.J. Freund, W.J. Wilson, Regression analysis : statistical modeling of a response variable, Academic Press, San Diego, 1998.
[53] S. Aburatani, K. Goto, S. Saito, H. Toh, K. Horimoto, ASIAN: a web server for inferring a regulatory network framework from gene expression profiles, Nucleic Acids Res. 33 (2005) W659–W664.

JVI
Journals.ASM.org

MicroRNA-27a Regulates Lipid Metabolism and Inhibits Hepatitis C Virus Replication in Human Hepatoma Cells

Takayoshi Shirasaki,[a,b] Masao Honda,[a,b] Tetsuro Shimakami,[a] Rika Horii,[a] Taro Yamashita,[a] Yoshio Sakai,[a] Akito Sakai,[a] Hikari Okada,[a] Risa Watanabe,[b] Seishi Murakami,[a] MinKyung Yi,[c] Stanley M. Lemon,[d] Shuichi Kaneko[a]

Department of Gastroenterology, Kanazawa University Graduate School of Medical Science, Kanazawa, Japan[a]; Department of Advanced Medical Technology, Kanazawa University Graduate School of Health Medicine, Kanazawa, Japan[b]; Human Center for Hepatitis Research, Institute for Human Infections and Immunity, and Department of Microbiology and Immunology, University of Texas Medical Branch, Galveston, Texas, USA[c]; Division of Infectious Diseases, School of Medicine, The University of North Carolina at Chapel Hill, Chapel Hill, North Carolina, USA[d]

The replication and infectivity of the lipotropic hepatitis C virus (HCV) are regulated by cellular lipid status. Among differentially expressed microRNAs (miRNAs), we found that miR-27a was preferentially expressed in HCV-infected liver over hepatitis B virus (HBV)-infected liver. Gene expression profiling of Huh-7.5 cells showed that miR-27a regulates lipid metabolism by targeting the lipid synthetic transcription factor RXRα and the lipid transporter ATP-binding cassette subfamily A member 1. In addition, miR-27a repressed the expression of many lipid metabolism-related genes, including *FASN*, *SREBP1*, *SREBP2*, *PPARα*, and *PPARγ*, as well as *ApoA1*, *ApoB100*, and *ApoE3*, which are essential for the production of infectious viral particles. miR-27a repression increased the cellular lipid content, decreased the buoyant density of HCV particles from 1.13 to 1.08 g/cm^3, and increased viral replication and infectivity. miR-27a overexpression substantially decreased viral infectivity. Furthermore, miR-27a enhanced *in vitro* interferon (IFN) signaling, and patients who expressed high levels of miR-27a in the liver showed a more favorable response to pegylated IFN and ribavirin combination therapy. Interestingly, the expression of miR-27a was upregulated by HCV infection and lipid overload through the adipocyte differentiation transcription factor C/EBPα. In turn, upregulated miR-27a repressed HCV infection and lipid storage in cells. Thus, this negative feedback mechanism might contribute to the maintenance of a low viral load and would be beneficial to the virus by allowing it to escape host immune surveillance and establish a persistent chronic HCV infection.

MicroRNA (miRNA) is a small, endogenous, single-stranded, noncoding RNA consisting of 20 to 25 bases that regulates gene expression. It plays an important role in various biological processes, including organ development, differentiation, and cellular death and proliferation, and is also involved in infection and diseases such as cancer (1).

Previously, we examined miRNA expression in hepatocellular carcinoma (HCC) and noncancerous background liver tissue infected with hepatitis B virus (HBV) and HCV (2). We showed that some miRNAs were differentially expressed according to HBV or HCV infection but not according to the presence of HCC. These infection-specific miRNAs were believed to regulate HBV or HCV replication; however, their functional role has not been elucidated.

HCV is described as a lipotropic virus because of its association with serum lipoprotein (3–5). It utilizes the low-density lipoprotein (LDL) receptor for cellular entry (6–8) and forms replication complexes on lipid rafts (9). The HCV core protein surrounds and binds lipid droplets (LDs) and nonstructural proteins on the endoplasmic reticulum (ER) membrane, which is essential for particle formation (10). Moreover, HCV cellular secretion is linked to very LDL (VLDL) secretion (11). In liver tissue histology, steatosis is often observed in chronic hepatitis C (CH-C) and is closely related to resistance to interferon (IFN) treatment (12, 13). Thus, lipids play important roles in HCV replication and CH-C pathogenesis.

Several miRNAs, such as miR-122 (14), miR-199a (15), miR-196 (16), miR-29 (17), Let-7b (18), and miR-130a (19), reportedly regulate HCV replication; however, miRNAs that regulate lipid metabolism and HCV replication have not been reported so far. Previously, we reported that 19 miRNAs were differentially expressed in HBV- and HCV-infected livers (2). In the present study, we evaluated the functional relevance of miR-27a in HCV replication by using the human hepatoma cell line Huh-7.5. We analyzed the regulation of lipid metabolism by miR-27a in hepatocytes and revealed a unique pathophysiological relationship between lipid metabolism and HCV replication in CH-C.

MATERIALS AND METHODS

Cell line. Huh-7.5 cells (kindly provided by C. M. Rice, Rockefeller University, New York, NY) were maintained in Dulbecco's modified Eagle's medium (DMEM; Gibco BRL, Gaithersburg, MD) containing 10% fetal bovine serum (FBS) and 1% penicillin-streptomycin.

HCV replication analysis. HCV replication analysis was performed by transfecting Huh-7.5 cells with JFH-1 (20), H77Sv2 Gluc2A (21), and their derivative RNA constructs. pH77Sv2 is a modification of pH77S, a plasmid containing the full-length sequence of the genotype 1a H77 HCV strain with five cell culture-adaptive mutations that promote its replication in Huh-7 hepatoma cells (21–24). pH77Sv2 Gluc2A is a related construct in which the *Gaussia* luciferase (Gluc) sequence, fused to the 2A autocatalytic protease of foot-and-mouth virus RNA, was inserted in frame between p7 and NS2 (21, 23, 25). pH77Sv2 Gluc2A (AAG) is a control plasmid that has an NS5B polymerase catalytic domain mutation.

Received 29 October 2012 Accepted 21 February 2013
Published ahead of print 28 February 2013
Address correspondence to Masao Honda, mhonda@m-kanazawa.jp.

doi:10.1128/JVI.03022-12

For RNA transfection, the cells were washed with phosphate-buffered saline (PBS) and resuspended in complete growth medium. The cells were then pelleted by centrifugation (1,400 × *g* for 4 min at 4°C), washed twice with ice-cold PBS, and resuspended in ice-cold PBS at a concentration of 7.5×10^6 cells/0.4 ml. The cells were mixed with 10 μg of the RNA transcripts, placed into 2-mm-gap electroporation cuvettes (BTX Genetronics, San Diego, CA), and electroporated with five pulses of 99 μs at 750 V over 1.1 s in an ECM 830 (BTX Genetronics). Following a 10-min recovery period, the cells were mixed with complete growth medium and plated.

miR-27a and anti-miR-27a transfection. Huh-7.5 cells transfected with pH77Sv2 Gluc2A RNA or pH77Sv2 Gluc2A (AAG) RNA were transfected with 50 nM synthetic miRNA (pre-miRNA) or 50 nM anti-miRNA (Ambion Inc., Austin, TX) with the siPORTTM NeoFXTM Transfection Agent (Ambion). Transfection was performed immediately by mixing the electroporated cells with the miRNA transfection reagents. Control samples were transfected with an equal concentration of a nontargeting control (pre-miRNA negative control) or inhibitor negative control (anti-miRNA negative control) to assess non-sequence-specific effects in the miRNA experiments.

Fatty acid treatment. Huh-7.5 cells transfected with HCV RNA and pre- or anti-miRNA were cultured for 24 h and then treated with the indicated concentrations of oleic acid (0 to 250 μM) (26) in the presence of 2% free fatty acid (FFA)-free bovine serum albumin (BSA; Sigma-Aldrich, St. Louis, MO). The cells were harvested at 72 h posttreatment with oleic acid for quantitative real-time detection PCR (RTD-PCR), Western blotting, immunofluorescence staining, and reporter analysis. The number of viable cells was determined by an MTS assay [one-step 3-(4,5-dimethylthiazol-2-yl)-2,5-diphenyltetrazolium bromide assay; Promega Corporation, Madison, WI]. Cellular triglyceride (TG) and cholesterol (TCHO) contents were measured with TG Test Wako and Cholesterol Test Wako kits (Wako, Osaka, Japan) according to the manufacturer's instructions.

Equilibrium ultracentrifugation of JFH-1 particles in isopycnic iodixanol gradients. Filtered supernatant fluids collected from JFH-1 RNA- and pre-miRNA- or anti-miRNA-transfected cell cultures were concentrated 30-fold with a Centricon PBHK Centrifugal Plus-20 filter unit with an Ultracel PL membrane (100-kDa exclusion; Merck Millipore, Billerica, MA) and then layered on top of a preformed continuous 10 to 40% iodixanol (OptiPrep; Sigma-Aldrich) gradient in Hanks' balanced salt solution (Invitrogen, Carlsbad, CA) as described previously (24). The gradients were centrifuged in an SW41 rotor (Beckman Coulter Inc., Brea, CA) at 35,000 rpm for 16 h at 4°C, and the fractions (500 μl each) were collected from the top of the tube. The density of each fraction was determined with a digital refractometer (Atago, Tokyo, Japan).

Infectivity assays. Huh-7.5 cells were seeded at 5.0×10^4/well in 48-well plates 24 h before inoculation with 100 μl of the gradient fractions. The cells were tested for the presence of intracellular core antigen by immunofluorescence 72 h later, as described below. Clusters of infected cells that stained for the core antigen were considered to constitute a single infectious focus, and virus titers were calculated accordingly in terms of numbers of focus-forming units (FFU)/ml.

Western blotting and immunofluorescence staining. Western blotting was performed as described previously (27). The cells were washed in PBS and lysed in radioimmunoprecipitation assay buffer containing Complete protease inhibitor cocktail and PhosSTOP (Roche Applied Science, Indianapolis, IN). The membranes were blocked in Blocking One or Blocking One-P solution (Nacalai Tesque, Kyoto, Japan), and the expression of HCV core protein, retinoid X receptor alpha (RXRα), sterol regulatory element-binding protein (SREBP1), ATP-binding cassette subfamily A member 1 (ABCA1), ApoE3, ApoB100, fatty acid synthase (FASN), peroxisome proliferator-activated receptor α (PPARα), ApoA1, phospho-PKR-like ER kinase (phospho-PERK), PERK, phospho-eIF2α, eIF2α, BIP, phospho-STAT1, and β-actin was evaluated with mouse anti-core (Thermo Fisher Scientific Inc., Rockford, IL), rabbit anti-RXRα, rabbit anti-SREBP1 (Santa Cruz Biotechnology Inc., Santa Cruz, CA), mouse anti-ABCA1 (Abcam, Cambridge, MA), goat anti-ApoE3, goat anti-ApoB100 (R&D Systems Inc., Minneapolis, MN), rabbit anti-FASN, rabbit anti-PPARα, mouse anti-ApoA1, rabbit anti-phospho-PERK, rabbit anti-PERK, rabbit anti-phospho-eIF2α, rabbit anti-eIF2α, rabbit anti-BIP, rabbit anti-phospho-STAT1, and rabbit anti-β-actin antibodies (Cell Signaling Technology Inc., Danvers, MA), respectively.

For immunofluorescence staining, the cells were washed twice with PBS and fixed in 4% paraformaldehyde for 15 min at room temperature. After washing again with PBS, the cells were permeabilized with 0.05% Triton X-100 in PBS for 15 min at room temperature. They were then incubated in a blocking solution (10% FBS and 5% BSA in PBS) for 30 min and with the anti-core monoclonal antibodies. The fluorescent secondary antibodies were Alexa 568-conjugated anti-mouse IgG antibodies (Invitrogen). Nuclei were labeled with 4′,6-diamidino-2-phenylindole (DAPI), and LDs were visualized with boron-dipyrromethene (BODIPY) 493/503 (Invitrogen). Imaging was performed with a CSU-X1 confocal microscope (Yokogawa Electric Corporation, Tokyo, Japan).

Quantitative RTD-PCR. Total RNA was isolated with a GenElute Mammalian Total RNA Miniprep kit (Sigma-Aldrich), and cDNA was synthesized with a high-capacity cDNA reverse transcription kit (Applied Biosystems, Carlsbad, CA). The primer pairs and probes for C/EBPα, ABCA1, PPARγ, SREBF1, SREBF2, FASN, 2′-5′-oligoadenylate synthetase 2 (OAS2), and β-actin were obtained from the TaqMan assay reagent library. HCV RNA was detected as described previously (28). HCV RNA was isolated from viral particles with a QIAamp viral RNA kit (Qiagen, Inc., Valencia, CA) in accordance with the manufacturer's instructions. Total RNA containing miRNA was isolated according to the protocol of the mirVana miRNA isolation kit (Ambion). For the enrichment of mature miRNA, argonaute 2 (Ago2)-binding miRNA was immunoprecipitated with an anti-Ago2 monoclonal antibody (Wako) and mature miRNA was eluted from the precipitant with a microRNA isolation kit, Human Ago2 (Wako). cDNA was prepared via reverse transcription with 10 ng of isolated total RNA and 3 μl of each reverse transcription primer with specific loop structures. Reverse transcription was performed with a TaqMan MicroRNA reverse transcription kit (Applied Biosystems) according to the manufacturer's protocol. RTD-PCR was performed with the 7500 Real Time PCR system (Applied Biosystems) according to the manufacturer's instructions. The primer pairs and probes for miR-let7a, miR-34c, miR-142-5p, miR-27a, miR-23a, and RNU6B were obtained from the TaqMan assay reagent library.

3′ UTR luciferase reporter assays. The miRNA expression reporter vector pmirGLO Dual-Luciferase miRNA Target Expression Vector (Promega Corporation) was used to validate the RXRα and ABCA1 3′ untranslated regions (UTRs) as miRNA binding sites. cDNA fragments corresponding to the entire 3′ UTR of human RXRα and human ABCA1 were amplified with the Access RT-PCR system (Promega Corporation) from total RNA extracted from Huh-7.5 cells. The PCR products were cloned into the designated multiple cloning site downstream of the luciferase open reading frame between the SacI and XhoI restriction sites of the pCR2.1-TOPO vector (Invitrogen). Point mutations in the seed region of the predicted miR-27a sites within the 3′ UTR of human RXRα and human ABCA1 were generated with a QuikChange Multi site-directed mutagenesis kit (Agilent Technologies Inc., Santa Clara, CA) according to the manufacturer's protocol. All constructs were confirmed by sequencing.

Huh-7.5 cells were grown to 70% confluence in 24-well plates in complete DMEM. The cells were cotransfected with 200 ng of the indicated 3′ UTR luciferase reporter vector and 50 nM synthetic miRNA (pre-miRNA) or 50 nM anti-miRNA (Ambion) in a final volume of 0.5 ml with Lipofectamine 2000 (Invitrogen). At 24 h posttransfection, firefly and *Renilla* luciferase activities were measured consecutively with the Dual-Luciferase Reporter Assay system (Promega Corporation).

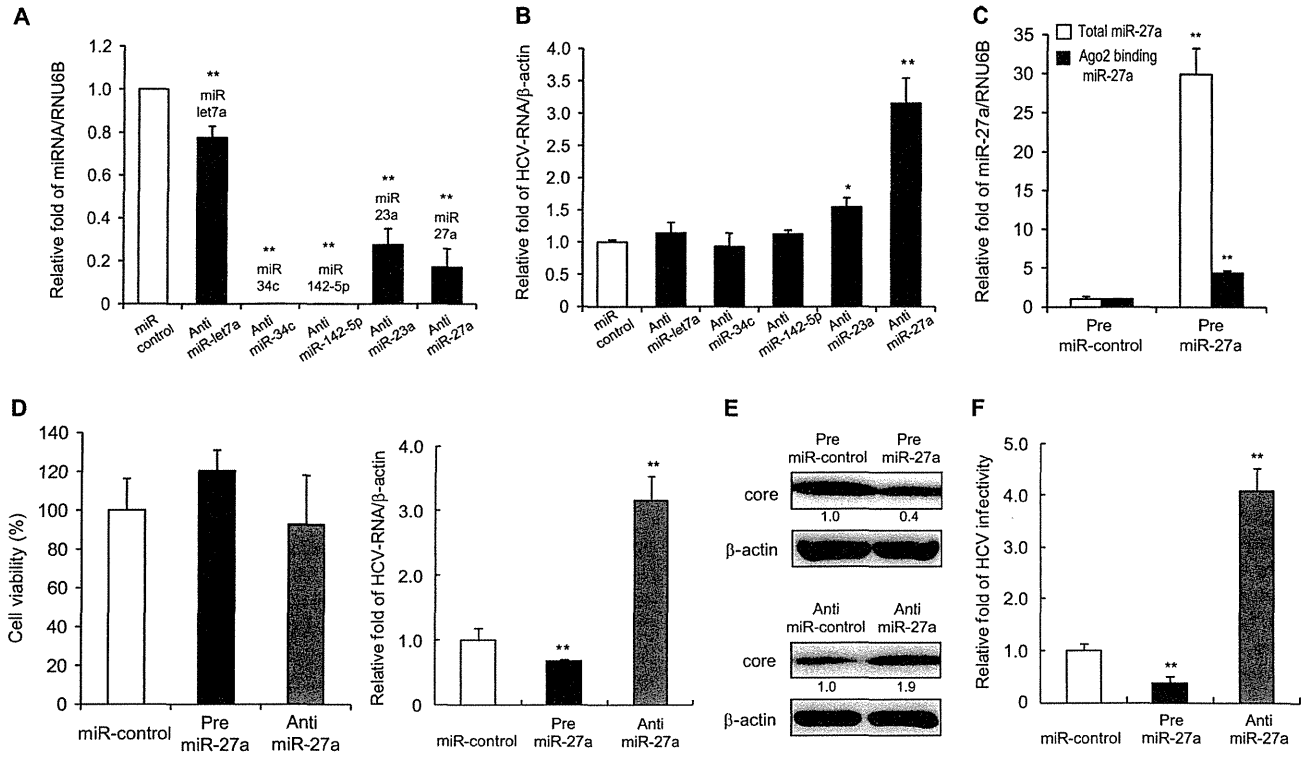

FIG 1 miR-27a has a negative effect on HCV replication and infectivity. Huh-7.5 cells were transfected with JFH-1 RNA and pre- or anti-miRNA. Expression was quantified at 72 h posttransfection. (A) Inhibition efficiency of miRNAs by anti-miRNAs (RTD-PCR, $n = 6$). (B) Effects of anti-miRNAs on HCV replication (RTD-PCR, $n = 6$). (C) Detection of whole miR-27a and Ago2-binding miR-27a in Huh-7.5 cells. At 72 h posttransfection, cells were harvested and Ago2-binding miRNA was purified as described in Materials and Methods. White bars indicate total miR-27a levels, and black bars indicate Ago2-binding miR-27a levels (RTD-PCR, $n = 6$). (D) Effects of pre- or anti-miR-27a on cell viability (left) and HCV replication (right). Cell viability (%) was assessed by the MTS assay ($n = 6$). (E) Effects of pre- or anti-miR-27a on HCV core protein levels by Western blotting. (F) Effects of pre- or anti-miR-27a on HCV infection. Huh-7.5 cells were infected with HCVcc derived from Huh-7.5 cells transfected with pre- or anti-miR-27a and JFH-1 RNA. HCV RNA was quantified at 72 h postinfection by RTD-PCR ($n = 6$). All experiments were performed in duplicate and repeated three times. Values are means ± standard errors. *, $P < 0.01$; **, $P < 0.005$.

Promoter analysis. DNA fragments from −400 to +36 bp and from −700 to +36 bp relative to the transcription initiation site of pri-miR-23a~27a~24-2 were inserted into pGL3-Basic (Promega Corporation) at the MluI and XhoI sites. Point mutations in the seed region of predicted C/EBPα binding sites were generated with a QuikChange Multi site-directed mutagenesis kit (Agilent Technologies) according to the manufacturer's protocol. All constructs were confirmed by sequencing.

Huh-7.5 cells transfected with HCV RNA were cultured for 24 h in 24-well plates, and then 200 ng of the plasmids was cotransfected with 2 ng of the *Renilla* luciferase expression vector (pSV40-Renilla) with the FuGENE6 Transfection Reagent (Roche Applied Science). After 24 h, the cells were treated with oleic acid in the presence of 2% FFA-free BSA (Sigma-Aldrich). At 48 h posttreatment, a luciferase assay was carried out with the Dual-Luciferase Reporter Assay system (Promega Corporation) according to the manufacturer's instructions.

For tunicamycin treatment, the plasmids (200 ng) were cotransfected with 2 ng pSV40-Renilla with FuGENE6 (Roche Applied Science) into Huh-7.5 cells grown in the wells of 24-well plates. After 24 h, the cells were treated for a further 24 h with the indicated concentrations of tunicamycin and a luciferase assay was carried out as described above.

RNA interference. A small interfering RNA (siRNA) specific to ABCA1 and a control siRNA were obtained from Thermo Fisher Scientific. Transfection was performed with Lipofectamine 2000 (Invitrogen) according to the manufacturer's instructions.

IFN treatment. Huh-7.5 cells transfected with HCV RNA and pre- or anti-miRNA were treated with oleic acid as described above. At 48 h later, the cells were treated with the indicated number of international units of IFN-α for 24 h.

Affymetrix GeneChip analysis. Aliquots of total RNA (50 ng) isolated from the cells were subjected to amplification with the WT-Ovation Pico RNA Amplification system (NuGen, San Carlos, CA) according to the manufacturer's instructions. The Affymetrix Human U133 Plus 2.0 microarray chip containing 54,675 probes has been described previously (29).

Statistical analysis. Results are expressed as mean values ± standard errors. At least six samples were tested in each assay. Significance was tested by one-way analysis of variance with Bonferroni methods, and differences were considered statistically significant at P values of <0.01 (*, $P < 0.01$; **, $P < 0.005$).

Microarray accession number. The expression data determined in this study were deposited in the Gene Expression Omnibus database (NCBI) under accession number GSE41737.

RESULTS

Functional relevance of the upregulated miRNAs in HCV-infected livers. Previously, 19 miRNAs were shown to be differentially expressed in HBV- and HCV-infected livers (2). Of these, 6 miRNAs were upregulated and 13 were downregulated. In this study, we focused on the upregulated miRNAs, as they might play a positive role in HCV replication. Anti-miRNAs and the control miRNA were transfected into Huh-7.5 cells following JFH-1 RNA

TABLE 1 Gene categories and names of differentially expressed genes regulated by miR-27a in Huh-7.5 cells

Protein function and name	Gene	Affy ID[a]	GB acc. no.[b]	Fold change		
				Pre-miR-27a/ miR-control	Anti-miR-27a/ anti-miR-control	Pre-miR-27a/ anti-miR-27a
Cytoskeleton remodeling and Wnt signaling						
Collagen, type IV, alpha 6	*COL4A6*	211473_s_at	U04845	0.85	2.19	2.58
Fibronectin 1	*FN1*	214702_at	AJ276395	0.57	1.14	2.02
Filamin A, alpha	*FLNA*	214752_x_at	AI625550	0.64	1.68	2.61
LIM domain kinase 1	*LIMK1*	204357_s_at	NM_002314	0.67	1.63	2.43
p21/Cdc42/Rac1-activated kinase 1	*PAK1*	230100_x_at	AU147145	0.63	1.58	2.53
Breast cancer anti-estrogen resistance 1	*BCAR1*	232442_at	AU147442	0.96	1.94	2.01
Frizzled homolog 3 (*Drosophila*)	*FZD3*	219683_at	NM_017412	0.51	1.30	2.55
Laminin, alpha 4	*LAMA4*	210990_s_at	U77706	0.63	1.26	2.00
Regulation of lipid metabolism						
CREB binding protein (Rubinstein-Taybi syndrome)	*CREBBP*	235858_at	BF507909	0.54	1.50	2.76
NF-Y	*NF-Y*	228431_at	AL137443	0.41	1.44	3.50
Sterol regulatory element binding transcription factor 2	*SREBF2*	242748_at	AA112403	0.47	1.11	2.35
Membrane-bound transcription factor peptidase, site 2	*MBTPS2*	1554604_at	BC036465	0.50	1.21	2.39
Adenosine A2A receptor signaling						
Mitogen-activated protein kinase kinase 7	*MAP2K7*	226053_at	AI090153	0.90	2.07	2.31
Par-6 partitioning defective 6 homolog beta	*PARD6B*	235165_at	AW151704	0.56	1.35	2.43
Rap guanine nucleotide exchange factor (GEF) 2	*RAPGEF2*	238176_at	T86196	0.46	1.36	2.98
Ribosomal protein S6 kinase, 90kDa, polypeptide 2	*RPS6KA2*	204906_at	BC002363	0.61	1.72	2.83
p53 regulation						
MDM2	*MDM2*	237891_at	AI274906	0.41	1.27	3.07
Ubiquitin B	*UBB*	217144_at	X04801	0.58	1.89	3.24
Promyelocytic leukemia	*PML*	235508_at	AW291023	0.52	1.45	2.80
SMT3 suppressor of mif two 3 homolog 1	*SUMO1*	208762_at	U83117	0.55	1.23	2.22
IL-8 in angiogenesis						
B-cell CLL/lymphoma 10	*BCL10*	1557257_at	AA994334	0.59	1.23	2.08
Janus kinase 2	*JAK2*	205841_at	NM_004972	0.77	1.71	2.23
Sphingosine-1-phosphate receptor 1						
G protein, alpha inhibiting activity polypeptide 2	*GNAI2*	201040_at	NM_002070	0.69	1.49	2.15
G protein, beta polypeptide 4	*GNB4*	223487_x_at	AW504458	0.86	1.78	2.06
Mitogen-activated protein kinase 1	*MAPK1*	1552263_at	NM_138957	0.87	1.93	2.22
GRB2-associated binding protein 1	*GAB1*	226002_at	AK022142	0.66	1.40	2.11

[a] Affy ID, Affymetrix identification number.
[b] GB acc. no., GenBank accession number.

transfection. The efficiency with which these anti-miRNAs inhibit the miRNAs is shown in Fig. 1A. Unexpectedly, inhibition of these miRNAs either had no effect or increased HCV replication in the cases of anti-miR-23a and anti-miR-27a (Fig. 1B).

To investigate the functional relevance of miR-27a in HCV replication in more detail, we evaluated JFH-1 replication in Huh-7.5 cells in which miR-27a was inhibited or overexpressed. The efficacy of miR-27a overexpression is shown in Fig. 1C. Although ectopically introduced pre-miR-27a increased miR-27a levels by approximately 30-fold, the levels of endogenous active Ago2 bound to miR-27a in RNA-induced silencing complexes increased by approximately 5-fold. The RNA and core protein levels of JFH-1 in Huh-7.5 cells decreased to 65% and 40%, respectively, following miR-27a overexpression. In contrast, the RNA and core protein levels of JFH-1 increased by 3- and 1.9-fold, respectively, following miR-27a inhibition (Fig. 1D and E). There was no significant difference in cell viability following miR-27a overexpression or inhibition (Fig. 1D). Furthermore, the rate of Huh-7.5 cell infection by JFH-1 decreased to 35% after the overexpression of miR-27a but increased 4-fold after miR-27a inhibition (Fig. 1F). Thus, miR-27a negatively regulates HCV replication and infection.

miR-27a targets the signaling pathways of cytoskeleton remodeling and lipid metabolism in Huh-7.5 cells. We next examined which signaling pathways were modulated by miR-27a. TargetScan (http://www.targetscan.org/) predicts biological targets of miRNAs by searching for the presence of conserved 8- and 7-mer sites that match the seed region of each miRNA (30). A TargetScan (release 5.2) for miR-27a predicted 921 candidate target genes, and functional gene ontology enrichment analysis of these genes by MetaCore (Thomson Reuters, New York, NY) showed that miR-27a could target the cytoskeleton remodeling and lipid metabolism signaling pathways (data not shown).

To examine whether these signaling pathways were regulated by miR-27a, gene expression profiling was carried out with Huh-7.5 cells in which miR-27a was over- or underexpressed. Transfection of cells with pre-miR-27a and pre-miR-

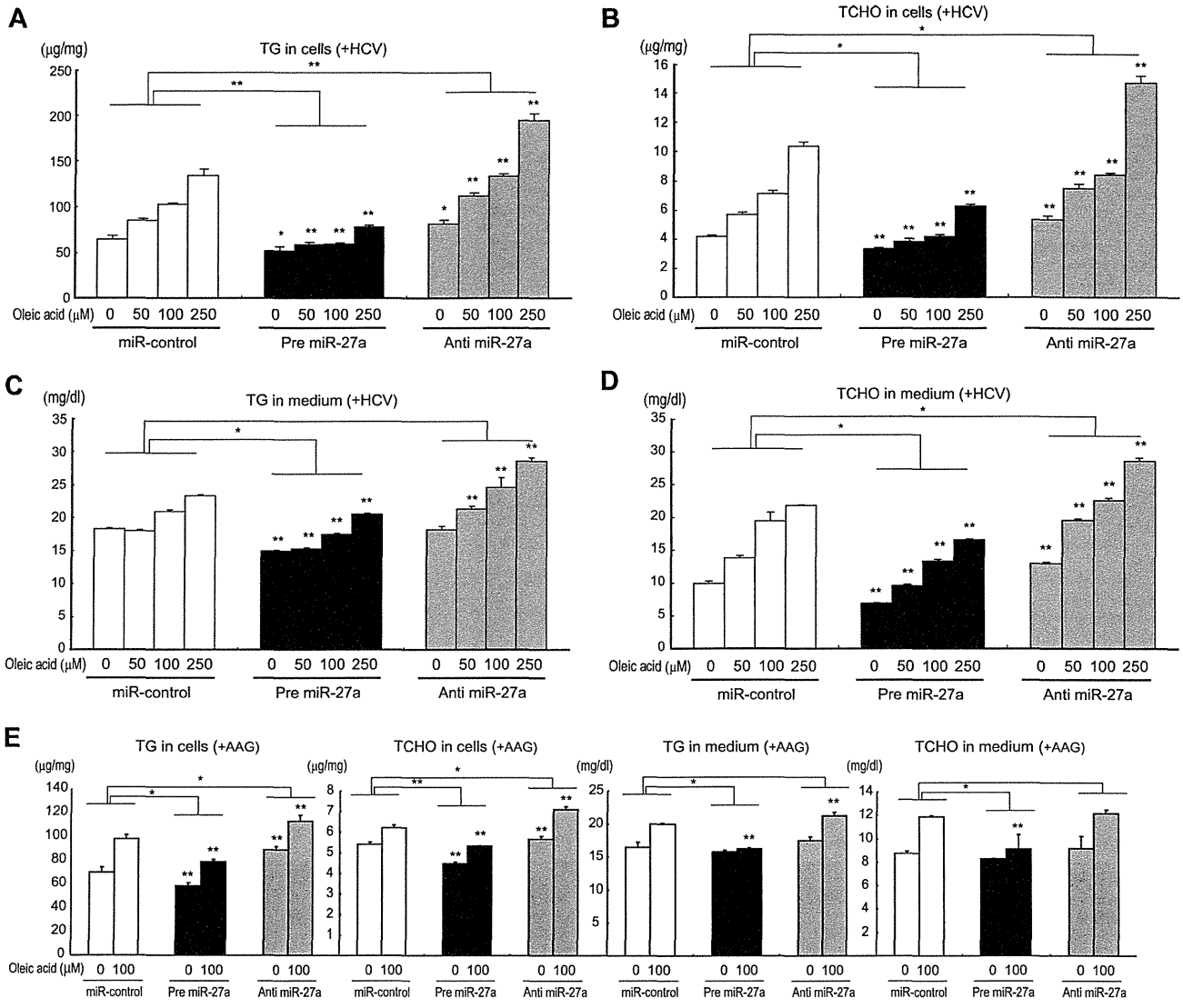

FIG 2 Changes in the lipid contents of Huh-7.5 cells and culture medium caused by pre- and anti-miR-27a. Huh-7.5 cells were transfected with replication-competent HCV RNA (H77Sv2 Gluc2A RNA [+HCV]) or replication-incompetent HCV RNA [H77Sv2 Gluc2A (AAG) (+AAG)] together with pre- or anti-miR-27a. At 24 h posttransfection, increasing amounts of oleic acid (0 to 250 μM) were added to the culture medium, and at 72 h after oleic acid treatment, TG and TCHO levels were measured in the cells and medium. Panels: A, TG in cells; B, TCHO in cells; C, TG in medium; D, TCHO in medium; E, TG and TCHO in cells and medium; A to D, +H77Sv2 Gluc2A (+HCV); E, +H77Sv2 Gluc2A (AAG) (+AAG). Lipid concentration was compared with that of miR-control and pre- or anti-miRNA ($n = 6$). All experiments were performed in duplicate and repeated three times. Values are means ± standard errors. *, $P < 0.01$; **, $P < 0.005$.

control or with anti-miR-27a and anti-miR-control enabled the identification of down- and upregulated genes, respectively. A total of 870 genes were selected with a >2-fold anti-miR-27a/pre-miR-27a expression ratio. Pathway analysis of these genes with MetaCore revealed that they are involved in cytoskeleton remodeling signaling, including that of *COL4A6*, *FN 1*, and *PAK1*; lipid metabolism signaling, including that of *CREBBP* and *SREBF2*; A2A receptor signaling, including that of *RAPGEF2*; and p53 regulation signaling, including that of *MDM2*. These genes were repressed by miR-27a in Huh-7.5 cells (Table 1).

miR-27a reduces TG and TCHO levels in cells and culture medium. Pathway analysis of the gene expression profile regulated by miR-27a in Huh-7.5 cells revealed the presence of many genes involved in lipid metabolism-related signaling pathways. To examine the functional relevance of miR-27a in lipid metabolism, we measured the cellular levels of TG and TCHO in Huh-7.5 cells in which miR-27a was inhibited or overexpressed, respectively. As shown in Fig. 2A and B, TG and TCHO levels in Huh-7.5 cells transfected with miR-control were increased in a dose-dependent manner following the addition of oleic acid (0 to 250 μM). Pre-miR-27a repressed this increase, while anti-miR-27a significantly accelerated it. Similarly, pre-miR-27a repressed the increase in TG and TCHO in the culture medium, while anti-miR-27a significantly accelerated it (Fig. 2C and D).

Similar results were obtained with both HCV-replicating cells

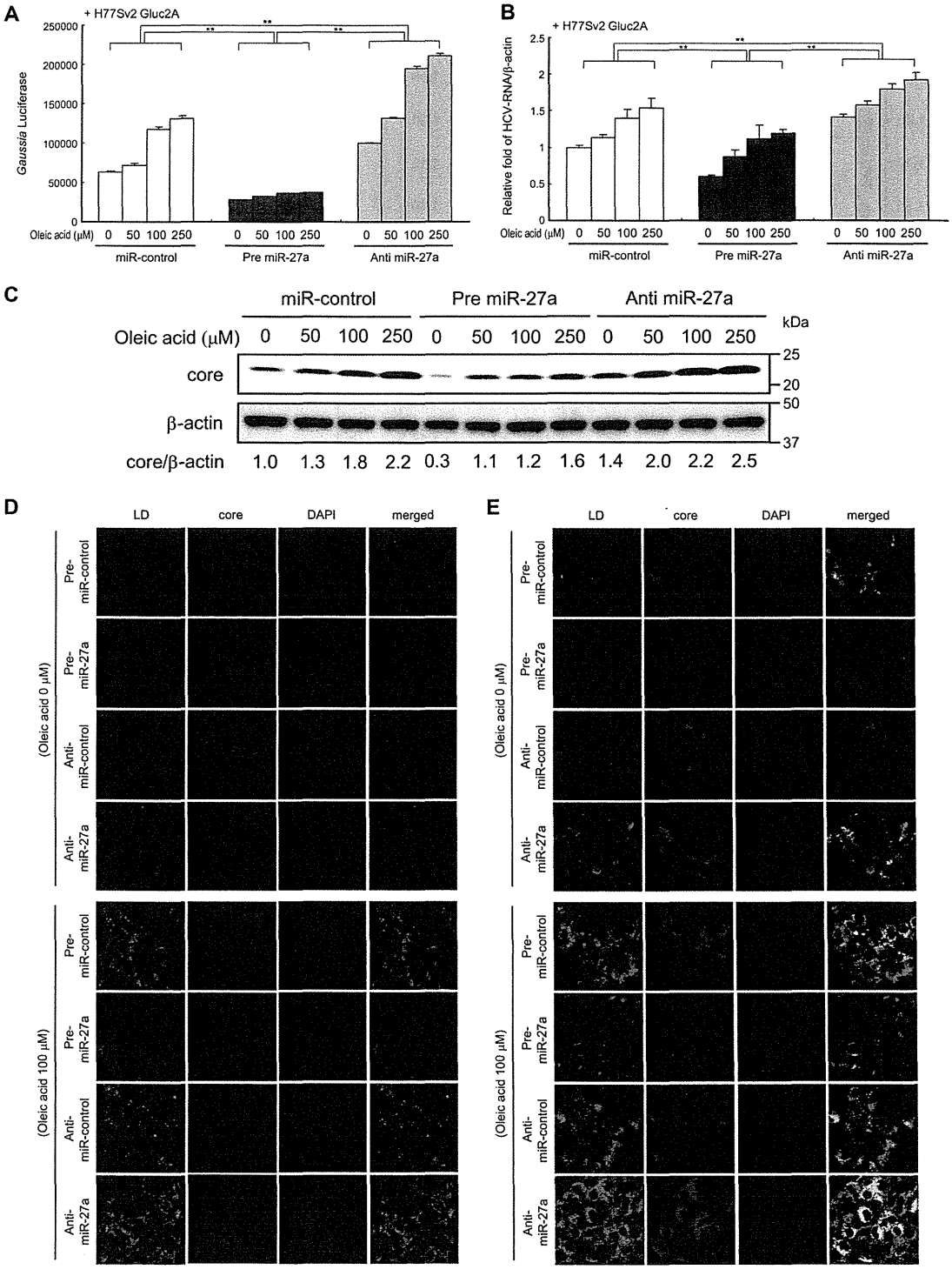

FIG 3 Changes in HCV replication in Huh-7.5 cells caused by pre- and anti-miR-27. Huh-7.5 cells were transfected with H77Sv2 Gluc2A RNA or H77Sv2 Gluc2A (AAG) RNA and pre- or anti-miR-27a. At 24 h posttransfection, increasing amounts of oleic acid (0 to 250 μM) were added to the culture medium. At 72 h after oleic acid treatment, the cells were harvested. (A) Gluc activity in the medium reflecting HCV replication in cells ($n = 6$). (B) Effects of pre- or anti-miR-27 on HCV RNA levels (RTD-PCR, $n = 6$). Experiments were performed in duplicate and repeated three times. Values are means ± standard errors. *, $P < 0.01$; **, $P < 0.005$. (C) Western blotting of HCV core protein in the same experiments. (D and E) Confocal microscopy images of Huh-7.5 cells in the same experiments. D, +H77Sv2 Gluc2A (AAG); E, +H77Sv2 Gluc2A. Cells were fixed, permeabilized, and stained with an anti-HCV core protein antibody. Nuclei were labeled with DAPI. LDs were visualized with BODIPY 493/503 dye. Imaging was performed with a CSU-X1 confocal microscope.

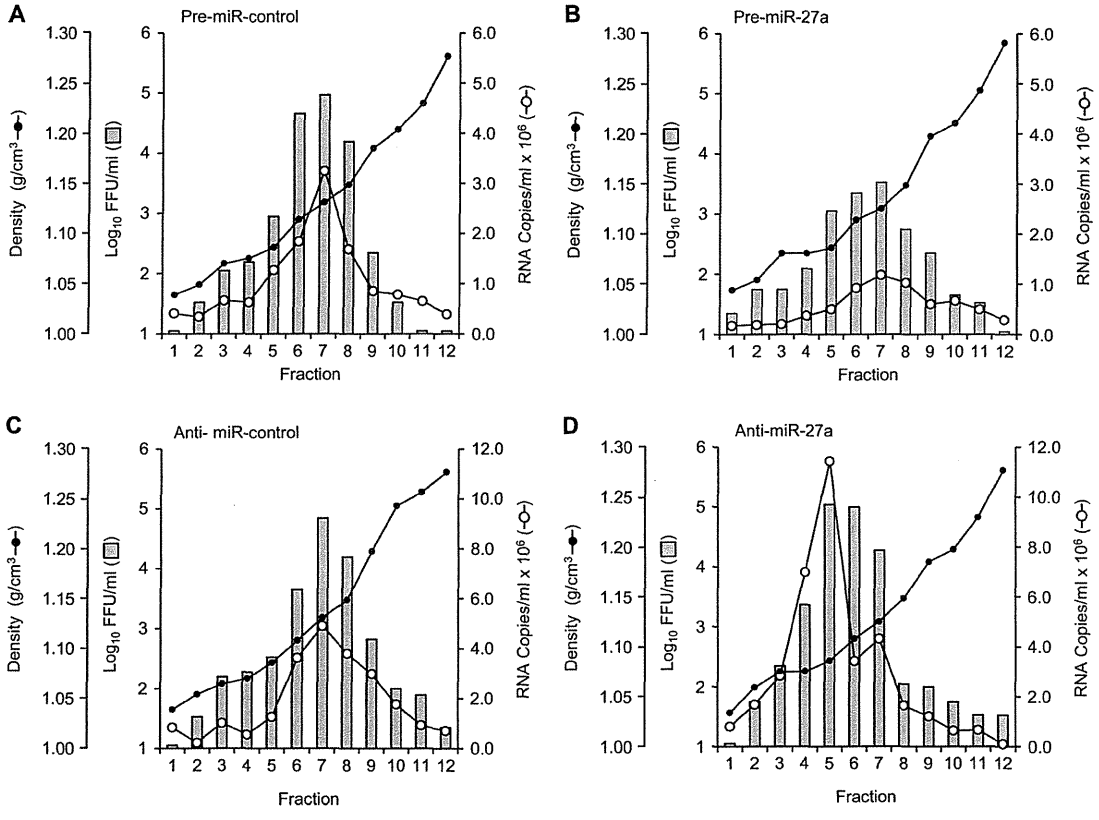

FIG 4 Equilibrium ultracentrifugation of JFH-1 particles in isopycnic iodixanol gradients. Filtered supernatant fluids collected from JFH-1 RNA- and pre- or anti-miRNA-transfected Huh-7.5 cell cultures were concentrated and used to collect fractions (500 μl each). Black circles indicate the gradient densities of the fractions, white circles indicate the HCV RNA titers, and bars indicate HCV infectivity levels. Panels: A, cells overexpressing pre-miR-control; B, cells overexpressing pre-miR-27a; C, cells overexpressing anti-miR-control; D, cells overexpressing anti-miR-27a. Experiments were repeated twice.

(+HCV) (Fig. 2A to D) and non-HCV-replicating cells (+AAG) (Fig. 2E), although the changes in the levels of TG and TCHO in the culture medium were smaller for the non-HCV-replicating cells (+AAG) (Fig. 2E). Correlating with the lipid component findings, replication of the infectious HCV clone H77Sv2 Gluc2A (21), as determined by Gluc activity in the culture medium, and the HCV RNA titer were significantly repressed by pre-miR-27a and increased by anti-miR-27a (Fig. 3A and B). This result was also confirmed by the core protein levels determined by Western blotting (Fig. 3C).

The localization of LDs and core proteins in the cells was visualized by confocal laser microscopy with a lipotropic fluorescent dye and immunostaining of the core protein (Fig. 3E). The LD and core protein levels were substantially repressed by pre-miR-27a and greatly increased by anti-miR-27a antibody. The change in the levels of LDs caused by miR-27a was observed in both HCV-replicating cells (Fig. 3E) and non-HCV-replicating cells (Fig. 3D), although the magnitude of the change was more prominent in HCV-replicating cells.

miR-27a changes the buoyant density and infectivity of HCV particles. The culture medium of Huh-7.5 cells in which JFH-1 was replicating was fractionated by iodixanol gradient centrifugation, and the buoyant density of HCV particles was evaluated (Fig. 4). When the cells were transfected with control miRNA (pre-miR-control and anti-miR-control), the HCV RNA titer (number of copies/ml) and infectivity (number of FFU/ml) peaked at fraction 7 (Fig. 4A and D) and the buoyant density of HCV was estimated at around 1.13 g/cm^3. Transfection with pre-miR-27a did not change the buoyant density of HCV, but it reduced the HCV RNA titer to 0.25-fold of the control and HCV infectivity to 0.024-fold of the control (Fig. 4B). In contrast, transfection with anti-miR-27a reduced the buoyant density of HCV from 1.13 to 1.08 g/cm^3 (Fig. 4B) and increased the HCV RNA titer to 2.1-fold of the control and infectivity to 2.5-fold of the control (Fig. 4C and D). Thus, miR-27a changed the buoyant density and infectivity of HCV.

miR-27a regulates lipid metabolism-related gene expression. The regulation of lipid metabolism-related genes by miR-27a was evaluated in Huh-7.5 cells (Fig. 5 and 6). The lipid synthesis transcription factors PPARγ, FASN, SREBP1, SREBP2, and RXRα were slightly, but significantly, induced in cells in which H77Sv2 Gluc2A replicated. The expression of lipid synthesis transcription factors was compared with that from cells carrying replication-incompetent H77Sv2 Gluc2A (AAG) (Fig. 5 and 6). Unexpectedly, lipid overload with oleic acid had no effect or rather decreased the levels of these transcription factors in non-HCV-replicating cells, probably because of negative feedback mechanisms. Conversely, in HCV-replicating cells, lipid overload with oleic acid further increased the levels of these transcription factors at both the

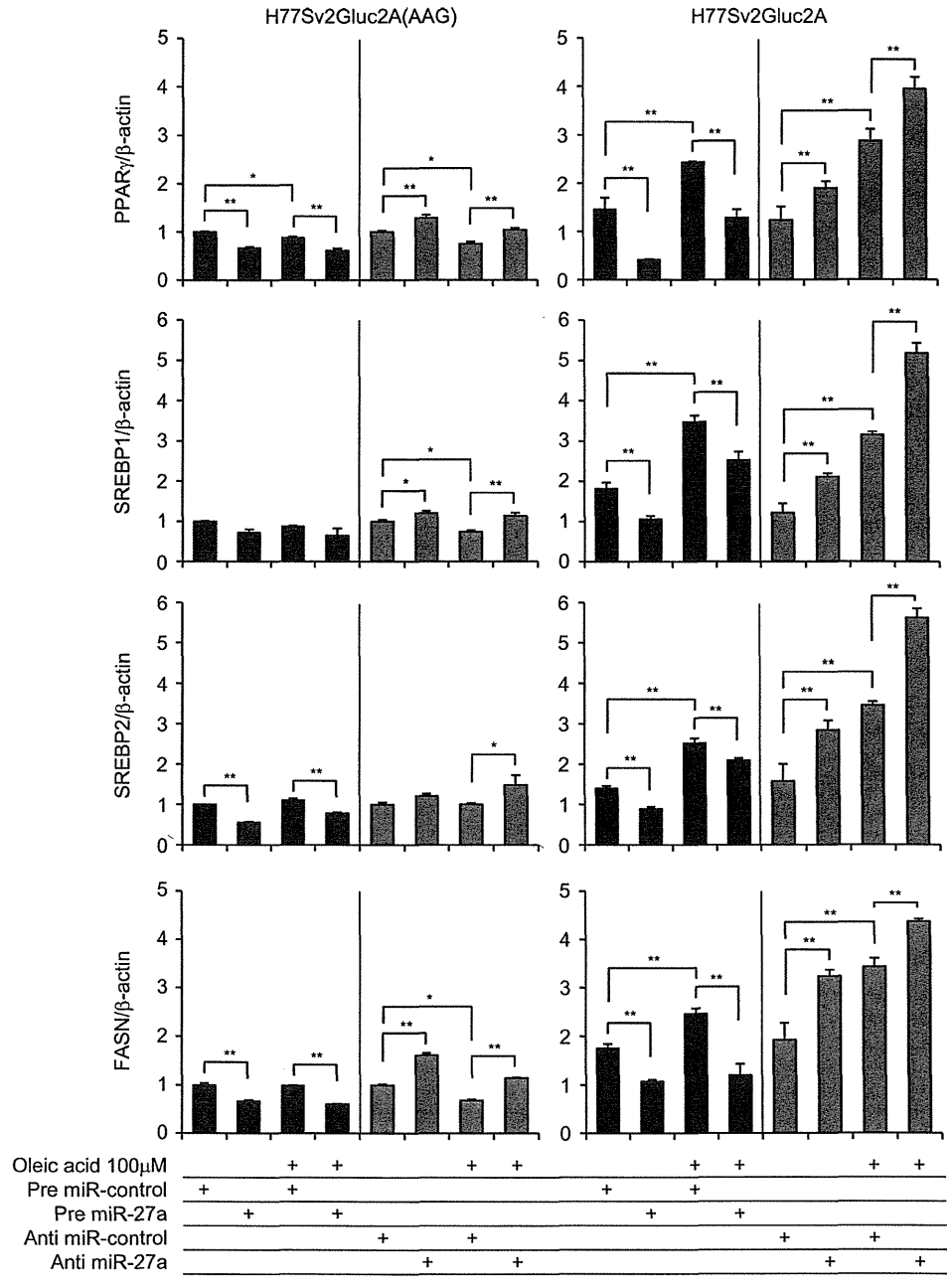

FIG 5 Expression of lipid metabolism-related transcription factors. Huh-7.5 cells were transfected with H77Sv2 Gluc2A RNA or H77Sv2 Gluc2A (AAG) RNA and pre- or anti-miR-27a. At 24 h posttransfection, oleic acid (100 μM) was added to the culture medium, and at 72 h after oleic acid treatment, *PPARγ*, *SREBP1*, *SREBP2*, and *FASN* expression levels were quantified by RTD-PCR ($n = 6$). Experiments were performed in duplicate and repeated three times. Values are means ± standard errors. *, $P < 0.01$; **, $P < 0.005$.

mRNA and protein levels (Fig. 5 and 6A and B). Pre-miR-27a significantly repressed the levels of these transcription factors and, conversely, anti-miR-27a significantly increased their mRNA and protein levels (Fig. 5 and 6A and B). This regulation by miR-27a was observed in both HCV-replicating and non-HCV-replicating cells, although the magnitude of the change was more prominent in HCV-replicating cells (Fig. 5).

As LDs associate with the ER-derived membrane at the site of HCV replication (10) and ER stress was recently shown to promote hepatic lipogenesis and LD formation (31), we next evaluated ER stress markers. Under HCV replication and lipid overload with oleic acid, anti-miR-27a increased the expression of the ER stress markers p-PERK, p-eIF2α, and BiP in Huh-7.5 cells. Conversely, pre-miR-27a significantly decreased the expression of these markers (Fig. 6C). Cell viability decreased after anti-miR-27a transfection and increased following pre-miR-27a treatment (Fig. 6D). Thus, miR-27a repressed the ER stress that was induced by HCV replication and lipid overload.

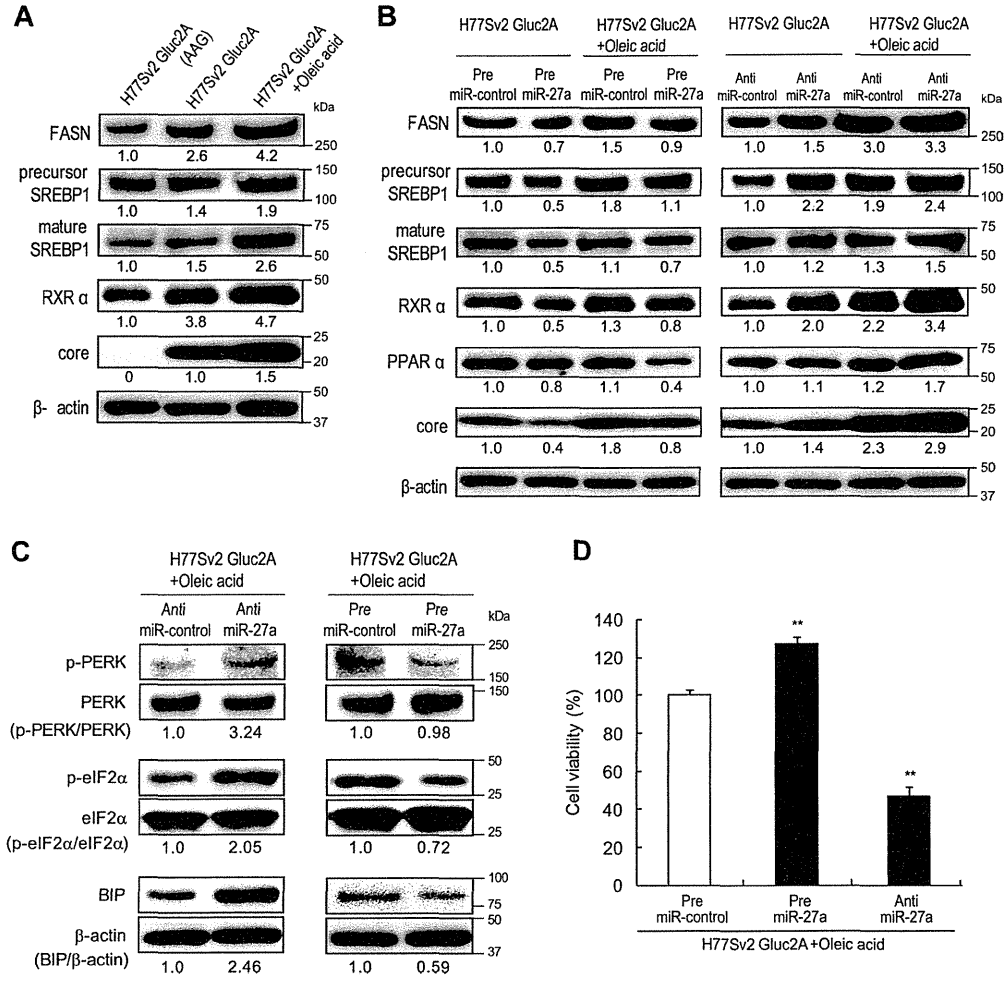

FIG 6 Expression of lipid metabolism-related transcription factors and ER stress-related factors. Huh-7.5 cells were transfected with H77Sv2 Gluc2A RNA or H77Sv2 Gluc2A (AAG) RNA and pre- or anti-miR-27a. At 24 h posttransfection, oleic acid (100 μM) was added to the culture medium. At 72 h after oleic acid treatment, the cells were harvested. (A) Western blotting of lipid metabolism-related transcription factors changed by HCV infection and oleic acid. Experiments were repeated three times. (B) Western blotting of lipid metabolism-related transcription factors changed by pre- or anti-miR-27a. Experiments were repeated three times. (C) Western blotting of ER stress-related transcription factors changed by pre- or anti-miR-27a. Experiments were repeated three times. (D) Cell viability in the same experiments was determined by MTS assay ($n = 9$). Experiments were performed in triplicate and repeated three times. Values are means ± standard errors. *, $P < 0.01$; **, $P < 0.005$.

miR-27a targets RXRα and the ATP-binding cassette transporter ABCA1. We next analyzed the expression of miR-27a target genes. A previous report showed that miR-27a targets RXRα in rat hepatic stellate cells (32), and we confirmed that miR-27a targets the 3′ UTR of human RXRα in Huh-7.5 cells (data not shown). Although the primary sequence of the human RXRα 3′ UTR shares approximately 60% homology with the corresponding rat sequence, the putative miR-27a binding site (ACUGUGAA) is conserved among several different species. Therefore, we constructed an expression vector containing a luciferase (Luc) reporter gene fused to the human RXRα 3′ UTR (pmirGLO-RXRα 3′ UTR) and reevaluated Luc activity (data not shown). Pre-miR-27a repressed Luc activity, while anti-miR-27a significantly increased Luc activity. The introduction of three nucleotide mutations into the conserved miR-27a binding site was shown to abolish these changes in Luc activity. These results confirmed previous findings that miR-27a targets RXRα (32). RXRα interacts with liver X receptor (LXR) and regulates many lipid synthetic genes such as *SREBP1* and *FASN*. We found that the expression of *SREBP1*, *FASN*, and *SREBP2* was regulated by miR-27a (Fig. 6B) and confirmed that *PPARγ* was also regulated by miR-27a, as reported previously (Fig. 5) (33). In addition, *PPARα* was shown to be regulated by miR-27a (Fig. 6B).

We next evaluated the expression of lipid transporter genes. The ATP-binding cassette transporter ABCA1 is mutated in Tangier's disease (34) and plays an important role in the efflux of TCHO for high-density lipoprotein (HDL) synthesis (35). A recent report demonstrated a functional role for ABCA1 in hepatocyte TG secretion to the plasma and in the reduction of cellular TG levels (29). Here we found that pre-miR-27a significantly repressed ABCA1 and, conversely, that anti-miR-27a increased the mRNA and protein levels of ABCA1 (Fig. 7A and B). We identified two miR-27a binding sites (sites 1 and 2) in the 3′ UTR of ABCA1 (Fig. 7C) that were conserved between species (Fig. 7C). An expression vector containing the *luc* reporter gene fused to the human ABCA1 3′ UTR (wild type [WT]) was constructed, and a

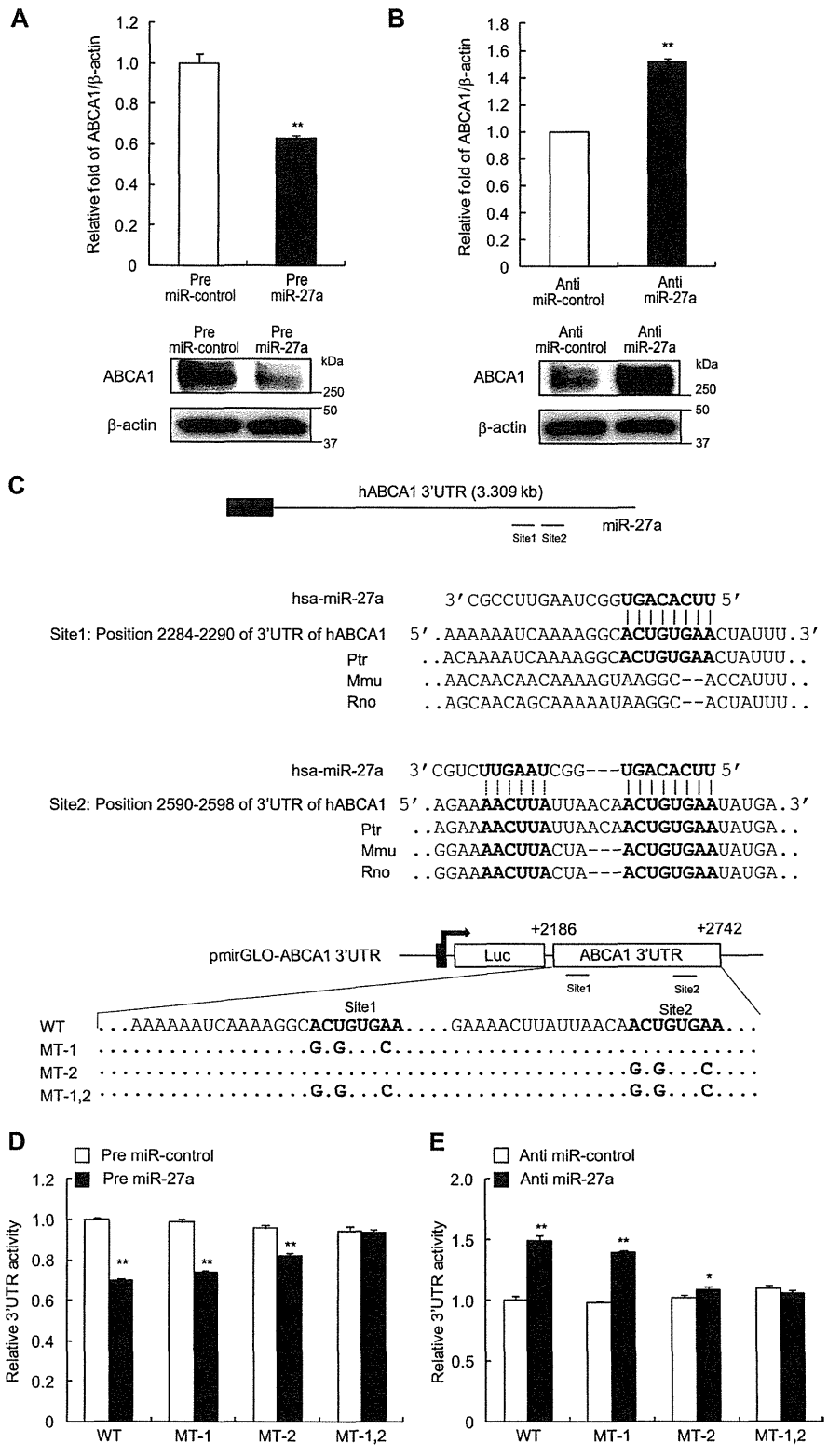

FIG 7 miR-27a targets ABCA1. (A) Regulation of ABCA1 by pre-miR-27a. RTD-PCR and Western blotting of ABCA1 in Huh-7.5 cells at 72 h posttransfection with pre-miR-control and pre-miR-27a ($n = 6$). **, $P < 0.005$. (B) Regulation of ABCA1 by anti-miR-27a. RTD-PCR and Western blotting of ABCA1 in Huh-7.5 cells at 72 h posttransfection with pre-miR-control and anti-miR-27a ($n = 6$). **, $P < 0.005$. (C) Sequence alignment of the ABCA1 3′ UTR and the construction of the luciferase (Luc) expression vector fused to the ABCA1 3′ UTR. Ptr, *Pan troglodytes*; Mmu, *Mus musculus*; Rno, *Rattus norvegicus*; WT, Luc reporter vector with the WT ABCA1 3′ UTR (2186 to 2742); MT-1, Luc reporter vector with the site 1 mutation of the WT; MT-2, Luc reporter vector with the site 2 mutation of the WT; MT-1,2, Luc reporter vector with mutations at sites 1 and 2 of the WT. (D, E) Suppression (D) or induction (E) of Luc activity with the various mutations of the ABCA1 3′ UTR by pre-miR-27a. Huh-7.5 cells were transfected with pre- or anti-miR-control or pre- or anti-miR-27a, and WT, MT-1, MT-2, and MT-1,2. Luc activities were measured at 24 h posttransfection ($n = 6$). All experiments were performed in duplicate and repeated three times. Values are means ± standard errors. *, $P < 0.01$; **, $P < 0.005$.

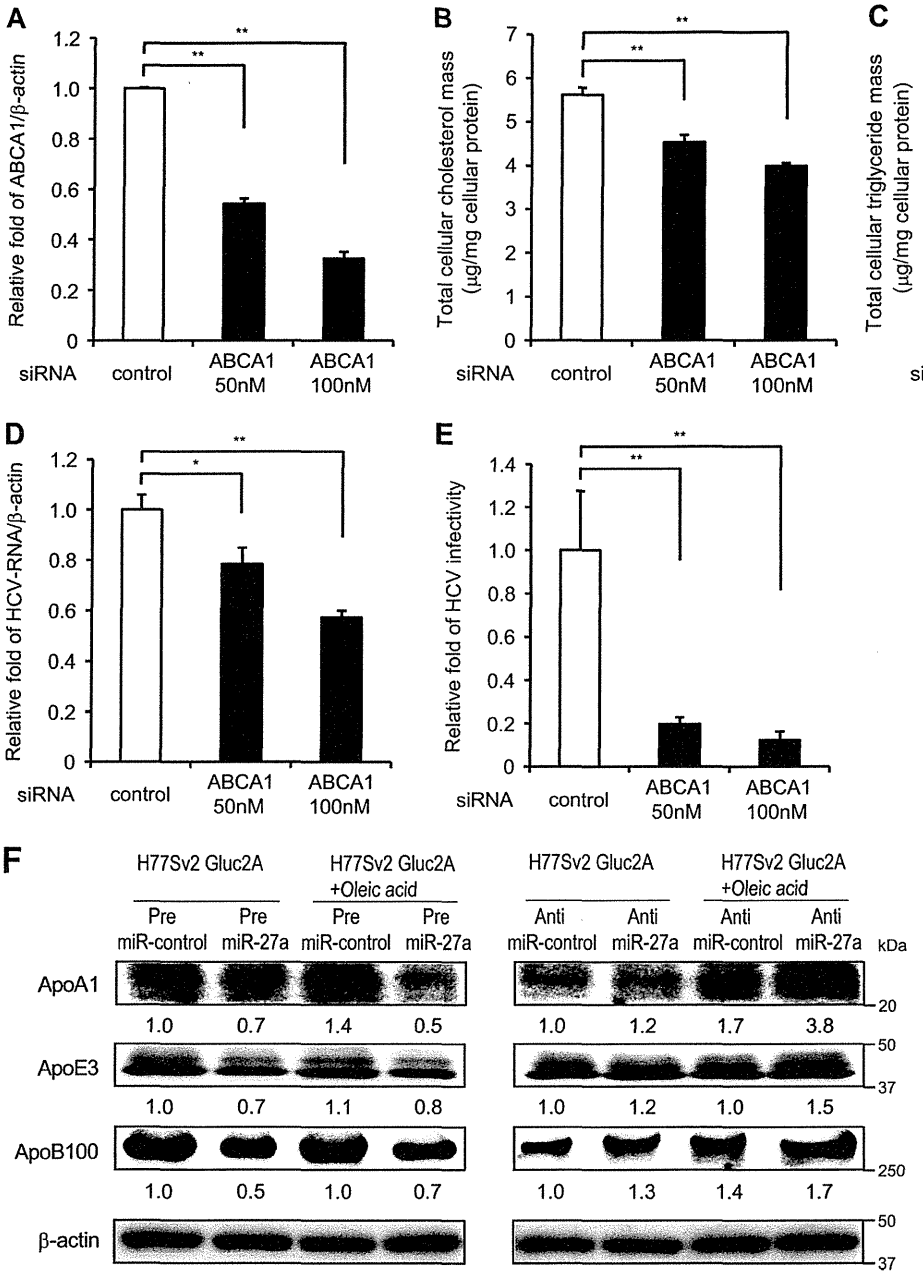

FIG 8 Suppression of ABCA1 inhibits HCV replication and infection. Huh-7.5 cells were transfected with H77Sv2 Gluc2A RNA and siRNA to ABCA1 or control siRNA. ABCA1 expression was quantified at 72 h posttransfection by RTD-PCR ($n = 6$). (A) Knockdown efficiency of ABCA1 in Huh-7.5 cells by siRNA. (B) TG concentration in cells ($n = 6$). (C) TCHO concentrations in cells ($n = 6$). (D) HCV RNA assay by RTD-PCR ($n = 6$). (E) HCV infectivity. Huh-7.5 cells were infected with HCVcc derived from ABCA1 knockdown Huh-7.5 cells. HCV RNA was quantified at 72 h postinfection by RTD-PCR ($n = 6$). Experiments were performed in duplicate and repeated three times. Values are means ± standard errors. *, $P < 0.01$; **, $P < 0.005$. (F) Regulation of ApoA1, ApoE2, and ApoB100 by miR-27a. Experiments were performed under the same conditions as Fig. 6B and C and repeated three times.

series of mutations were introduced into the putative miR-27a binding sites (MT-1, MT-2, and MT-1,2). The Luc activity of the WT was significantly repressed by pre-miR-27a and increased by anti-miR-27a. However, there was a smaller change in Luc activity caused by pre- and anti-miR-27a in the single mutants (MT-1 and MT-2) and no change in Luc activity in the double mutant (MT-1,2) (Fig. 7D and E). These results show that miR-27a targets ABCA1 to decrease the lipid content of cells.

The functional relevance of ABCA1 in lipid metabolism and HCV replication in Huh-7.5 cells was examined by inhibiting ABCA1 with an siRNA (Fig. 8). siRNA to ABCA1 repressed the expression of ABCA1 in a dose-dependent manner (Fig. 8A). Under this condition, the cellular TG and TCHO levels decreased significantly (Fig. 8B and C) and HCV RNA levels also decreased to 57% of the control. More strikingly, HCV infectivity decreased to 12% of the control (Fig. 8D and E).

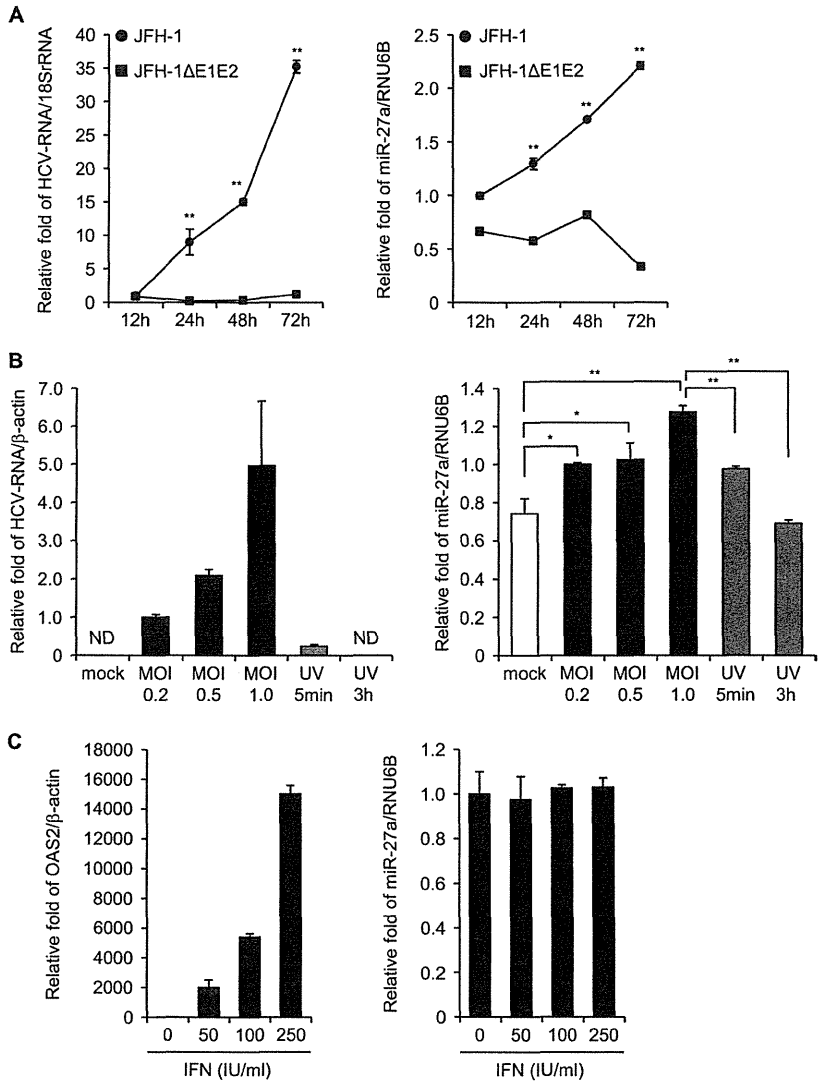

FIG 9 miR-27a is upregulated by HCV infection. (A) Kinetics of HCV replication and induction of miR-27a. Huh-7.5 cells were transfected with JFH-1 RNA or infection-incompetent JFH-1ΔE1E2 RNA (20). At 12, 24, 48, and 72 h posttransfection, HCV RNA (left) and miR-27a (right) levels were quantified by RTD-PCR ($n = 6$). (B) Induction of miR-27a and UV-irradiated HCV particles. Huh-7.5 cells were infected with infectious HCV (multiplicity of infection [MOI] of 0.2, 0.5, or 1) or UV-inactivated HCV. At 72 h postinfection, HCV RNA (left) and miR-27a (right) were quantified by RTD-PCR ($n = 6$). *, $P < 0.01$; **, $P < 0.005$; ND, not detected. (C) Induction of miR-27a and IFN-α treatment. Huh-7.5 cells were treated with different doses of IFN-α. At 24 h posttreatment, OAS2 (left) and miR-27a (right) were quantified by RTD-PCR ($n = 6$). All experiments were performed in duplicate and repeated three times. Values are means ± standard errors.

Several reports have demonstrated the importance of apolipoproteins, including the major components of VLDL and LDL apoE3 (36) and apoB100 (11), in the production of infectious HCV particles. More recently, the functional relevance of ApoA1 in HCV replication and particle production has been reported (37). Here the expression of apoA1, apoB100, and apoE3 was repressed by pre-miR-27a and increased by anti-miR-27a, suggesting that miR-27a regulates the expression of apolipoproteins to reduce the production of infectious HCV particles (Fig. 8F).

Regulation of miR-27a expression through C/EBPα. miR-27a forms a gene cluster with miR-23a and miR-24-2, and both of these miRNAs are regulated by the same promoter (38). However, no detailed analysis of the regulation of this promoter has been carried out. Because the expression of miR-27a was upregulated more in CH-C liver than CH-B liver, it could be speculated that HCV infection induces the expression of miR-27a. To examine this, we evaluated the expression of miR-27a during HCV infection (Fig. 9). The expression of miR-27a increased, correlating with the increase in JFH-1 RNA, while infection-incompetent JFH-1ΔE1E2 did not induce miR-27a expression (Fig. 9A). In addition, UV-irradiated HCV particles did not induce miR-27a expression (Fig. 9B). However, IFN-α treatment did not induce the expression of miR-27a (Fig. 9C). Thus, HCV infection was essential for induction of miR-27a expression.

We identified a C/EBPα binding site (−614 to −606), a key regulator of adipocyte differentiation, in the promoter region of miR-27a. Interestingly, H77Sv2 Gluc2A and tunicamycin